Biomaterials Science

REVIEW

View Article Online
View Journal | View Issue

Cite this: *Biomater. Sci.*, 2019, **7**, 2218

Microfluidics for silica biomaterials synthesis: opportunities and challenges

Nanjing Hao, Yuan Nie and John X. J. Zhang *

Received 13th February 2019,
Accepted 12th March 2019

DOI: 10.1039/c9bm00238c

rsc.li/biomaterials-science

The rational design and controllable synthesis of silica nanomaterials bearing unique physicochemical properties is becoming increasingly important for a variety of biomedical applications from imaging to drug delivery. Microfluidics has recently emerged as a promising platform for nanomaterial synthesis, providing precise control over particle size, shape, porosity, and structure compared to conventional batch synthesis approaches. This review summarizes microfluidics approaches for the synthesis of silica materials as well as the design, fabrication and the emerging roles in the development of new classes of functional biomaterials. We highlight the unprecedented opportunities of using microreactors in biomaterial synthesis, and assess the recent progress of continuous and discrete microreactors and the associated biomedical applications of silica materials. Finally, we discuss the challenges arising from the intrinsic properties of microfluidics reactors for inspiring future research in this field.

1. Introduction

Since the introduction of solid silica micro-/nanoparticles through the hydrolysis and condensation process of silicates under basic conditions by Stöber in 1968,[1] the past several decades have witnessed an explosive growth in the synthesis of silica materials especially from the discovery of porous silica particles in 1992.[2] Solid and porous silica materials with advanced features, such as good biocompatibility, high thermal and mechanical stability, and ease of surface functionalization, show great promise in numerous biological applications ranging from bioimaging, biosensors, and drug delivery, to disease theranostics.[3–8] Accompanying with the use of silica materials spreading from applications requiring large bulk quantities to niche biological applications, the requirements regarding the physicochemical properties of particulates including size, shape, porosity, and structure are becoming increasingly important and stringent.[9–11]

Over the years, a number of different synthetic methods based on conventional batch reactors have been developed for producing silica materials. Many of these methods, however, always suffer from issues of uniformity, yield, and batch-to-batch reproducibility arising from inadequate reaction control.[5,12–14] The advent of microfluidics in the 1990s opened a new realm of possibilities for chemical engineering in the confined space on a micrometer scale.[15–21] Microfluidics systems enable controllable and precise manipulation of process parameters (*e.g.* flow rate, residence time, temperature, and pressure), which provides a powerful platform for the continuous, scalable, and reproducible production of micro-/nanomaterials with unprecedented control over their size, shape, porosity, and structure properties. To date, microfluidics techniques have already fully demonstrated their remarkable capacity in the rational design and controllable synthesis of polymers,[22–26] quantum dots,[27,28] and metallic materials.[29,30] For the synthesis of silica materials through microfluidics reactors, although it is still in the preliminary stage, there have already been a range of important developments and breakthroughs by researchers including our group.

This review first discusses the recent progress of microfluidics for the synthesis and bioapplications of silica materials. Specifically, it is organized as follows: firstly, we highlight the unprecedented opportunities of using microfluidics reactors in the rational design and controllable synthesis of silica biomaterials compared with conventional batch reactors; secondly, we summarize the recent achievements of the microfluidics-enabled synthesis of solid and porous silica materials from continuous and discrete microreactors; then, we present the established bioapplications of silica materials from microreactors in the areas of bioimaging, protein immobilization, bioadsorption, drug delivery, and liquid biopsy; finally, we identify the challenges of microfluidics in silica biomaterials synthesis and propose future perspectives in this research field.

Thayer School of Engineering, Dartmouth College, 14 Engineering Drive, Hanover, New Hampshire 03755, USA. E-mail: john.zhang@dartmouth.edu

2. Beyond the batch reactor: why the microreactor matters

2.1 Microfluidics design parameters

Microreactors build upon microfluidics technology, which studies the science and technology of systems that manipulate micro- or nanoliter fluids and exploit their unique behaviors on a microscale.[18] The direct advantage of scaling down in dimensions is the high surface-to-volume ratio, which provides rapid heat and mass transfer in microreactors. Surface forces such as viscous forces dominate over inertial forces in microreactors. The ratio of the two is described by the Reynolds number (*Re*), which is a dimensionless number often used to estimate if the flow in microreactors is laminar or turbulent.[31] The expression for the Reynolds number is:

$$Re = \frac{\rho UL}{\mu}$$

where ρ is the density of the fluids (kg m^{-3}), U is the average velocity of the fluids (m s^{-1}), L is the characteristic length of the microchannel (m), and μ is the dynamic viscosity of the fluids (*Pa* s). The flow in microreactors is almost always laminar due to the microscale. This makes the flow very easily predictable: at a given point, velocity is constant. The governing equations of fluid dynamics in microreactors are the Navier–Stokes equations:[31]

$$\rho\left(\frac{\partial \bar{\mathbf{u}}}{\partial t} + \bar{\mathbf{u}} \cdot \nabla \bar{\mathbf{u}}\right) = -\nabla p + \mu \nabla^2 \bar{\mathbf{u}} + \bar{\mathbf{f}}$$

where $\bar{\mathbf{u}}$ is the velocity field, p is the pressure field, and $\bar{\mathbf{f}}$ is the force field. The Navier–Stokes equations can be simplified by assuming low Reynolds number, and incompressible and fully developed Newtonian fluids. With non-slip boundary conditions, a parabolic velocity profile can be obtained by solving the simplified equations. While the laminar flow allows for more controllable reactions in microreactors, it causes diffusion limited mixing of reagents. This can be addressed by designing passive or active mixing modules based on strategies such as chaotic advection or electrokinetics.[32] Design of microreactors for advanced mixing performance is guided by the Péclet number (*Pe*):[31]

$$Pe = \frac{UL}{D}$$

where U is the average velocity of the fluids (m s^{-1}), L is the characteristic length of the microchannel (m), and D is the diffusion coefficient (m^2 s^{-1}). The Péclet number compares the rate of advection (or transport by the fluids) to that of diffusion across the fluids. The scale of molecular diffusion coefficient is 10^{-10}–10^{-11} (m^2 s^{-1}),[33] the dimension of microchannels is 10^{-6}–10^{-4} (m), and a typical velocity in microchannels is ~1 (m s^{-1}); so, the Péclet number in microreactors is relatively large, and the effect of diffusion-induced mixing could even be neglected in some cases. For improved mixing, one strategy is to increase the length of microchannels by adding long winding channels.

2.2 Pressure-driven microreactors: laminar flow and discrete flow

Compared to conventional batch-mode reactors, microreactors have many superior properties: rapid heat and mass transfer ensures fast kinetic reactions, low volume of fluids results in low consumption of reagents and low cost, and predictable laminar flow offers a controllable synthesis process.[34] There are five groups of major microfluidics systems based on the main liquid propulsion principle: capillary-based, pressure driven, centrifugal, electrokinetic, and acoustic microfluidics platforms.[35] Pressure-driven microfluidics platforms have been chosen for chemical synthesis as they are easier to control and more flexible to design, not requiring any external fields. In this review, we mainly focus on pressure-driven microreactors unless otherwise stated. Pressure-driven microreactors can be further categorized into two main groups: single-phase continuous laminar flow and multi-phase discrete flow. As shown in Fig. 1, continuous laminar-flow microreactors are simply designed with multiple inlets for different reagents, an outlet for final reaction products and a mixing module to improve

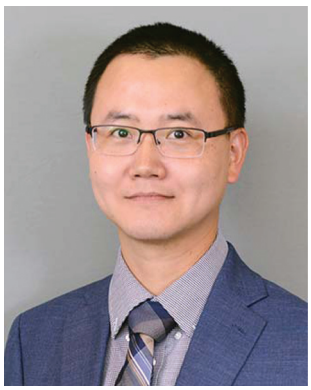

Nanjing Hao

Dr Nanjing Hao is currently a research associate at the Thayer School of Engineering, Dartmouth College, New Hampshire (NH), USA. He obtained his bachelor's degree in Bioengineering (2009) and PhD degree in Chemistry (2014) in P.R. China. His current research interest focusses on microfluidics-enabled on-chip colloidal materials synthesis for applications in liquid biopsy, biosensors, catalysis, and environment.

Yuan Nie

Yuan Nie received her BS degree (2011) and MS degree (2014) in Mechanical Engineering in P.R. China. She is currently a Ph.D. candidate at Thayer School of Engineering, Dartmouth College, NH, USA. Her research interests are on the development of microfluidics reactors, synthesis of nanomaterials, on-chip biosensing and cell analysis.

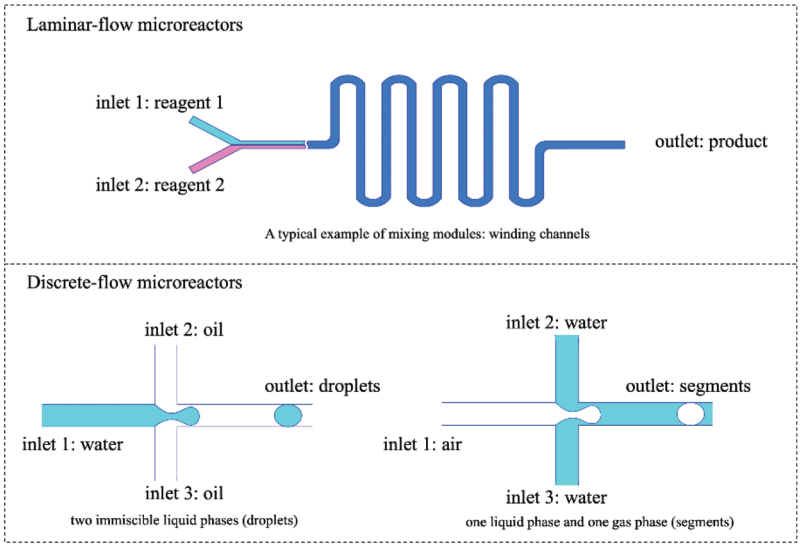

Fig. 1 Pressure-driven microreactors categorized into two main groups: continuous laminar-flow and discrete segmented-flow microreactors.

diffusion-limited mixing in microreactors. A typical example of mixing modules is winding channels.[32] Discrete flow microreactors include both liquid droplets and gas segments. Droplet microreactors involve two immiscible liquid phases such as water (reagent fluid) and silicone oil (carrier fluid) to generate droplets.[36] The compartmentalization provides an enclosed chamber where reagents can mix dramatically with each other. Droplet formation requires a specific "nozzle" design such as Y-shaped, T-shaped, or cross-shaped geometries.[37] The size of the droplets controls the size, morphology and monodispersity of the final reaction products. Another common type of discrete flow microreactor uses the gas phase to separate the "segments" of the reagents. This can be used to avoid any contaminations introduced by carrier fluids.

The workflows of both microreactors and batch-mode reactors are provided in Fig. 2. Operation in microreactors is simple and convenient: add reagents into syringes that connect to the inlets of microreactors, set the flow rate for each inlet flow, determine the target volume, wait until the reaction is complete, and collect the products at the outlet. During the procedure, manual operation is only required at the beginning and the very end. The process is programmable and automatic. The reaction rate can be tuned by changing the flow rate of reagents and by adjusting the reaction time. The geometry design of microreactors also offers flexibility towards the synthesis. In comparison, the procedure of conventional batch-mode reactors is very complicated, non-automatic, and not programmable. Each step demands human labor and careful operation such as dropwise addition of reagents. For a reaction that takes hours, watching over the whole process and adding different reagents at certain times is required, making the process extremely troublesome and time-consuming. Moreover, mixing of reagents relies on magnetic or mechanical stirring, which is not as efficient or complete as that at the microscale. The reaction rate can only be affected by the limited stirring rate. The conventional batch-mode reactors lack control over the synthesis process.

A comparison between microreactors (both laminar-flow and segmented-flow microreactors) and conventional batch-mode reactors is summarized in Table 1.[38] While batch-mode reactors require extra labor and effort, microreactors are very convenient to operate. In microreactors, we can easily adjust the parameters for the reaction including the geometry design of microreactors and flow rate. In batch-mode reactors, we can only change the stirring rate during the reaction, which does not really give us any control. Compared to batch-mode reactors, precise control over each step including seeding, growth

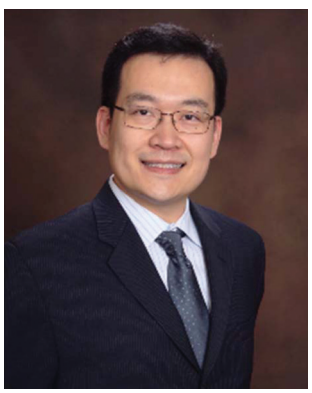

John X. J. Zhang

John X. J. Zhang is a Professor at the Thayer School of Engineering, Dartmouth College, NH, USA, and a Fellow of AIMBE. He received his PhD degree from Stanford University, CA, USA. His research is on developing miniature medical systems to improve global health, through innovations in bio-inspired nanomaterials, lab-on-chip design, and advanced nanofabrication technologies. He is a recipient of numerous prestigious awards, including the NSF CAREER award, DARPA Young Faculty Award, Wallace Coulter Foundation Early Career Award and NIH Director's Transformative Research Award. Dr Zhang has mentored over 30 Ph.D. students and post-doctoral scholars, and published a textbook in biomedical engineering.

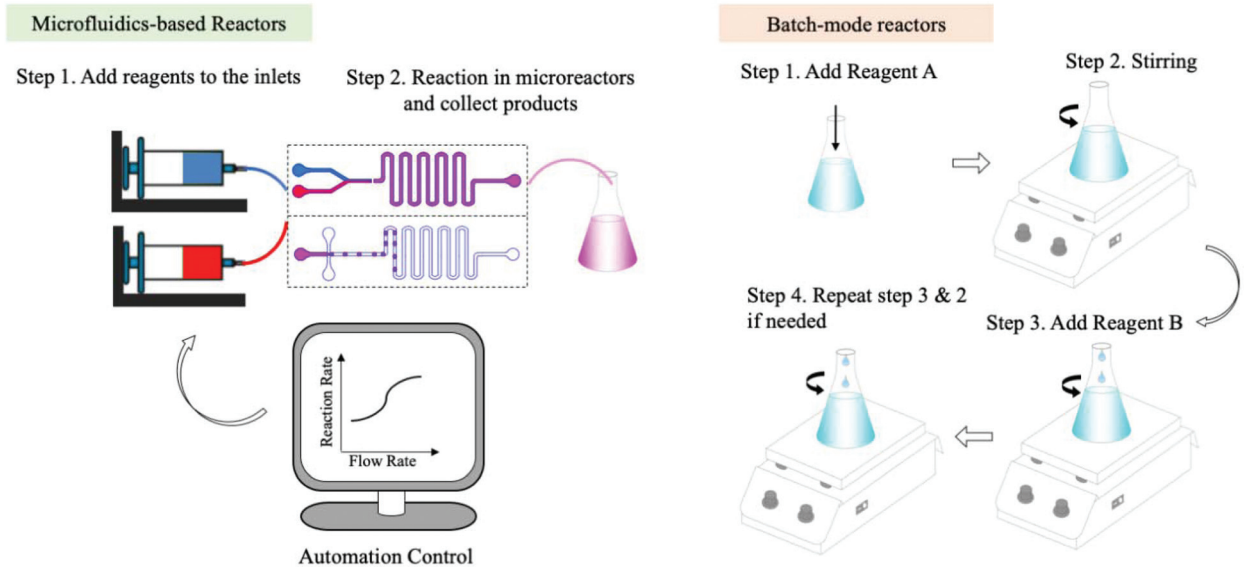

Fig. 2 Workflow of microfluidics-based reactors and batch-mode reactors (image not to scale).

Table 1 Comparison between microfluidics reactors and batch reactors

	Microfluidics reactors		
	Laminar flow	Discrete flow	Macroscopic batch reactors
Chip-scale operations	Yes	Yes	No
Tunable parameters	Yes, the design of microfluidics reactors and the adjustable flow rate provide flexible reactions		No, the only adjustable parameter may be the stirring rate during the reaction
Fast reaction	Yes, generally takes seconds or less		No, usually takes hours or days
Precise control	Yes, precise control over each step: seeding, growth and ceasing reaction		No, lack control over seeding and growth
Reproducibility	Medium	High	Low
Automation	Yes, programmable equipment makes the process automatic		No, usually require watching over the process
Low consumption of reagents	Yes, owing to the scale effect		No
Scale-up probability	Low	Moderate	High, very easy to fabricate large quantity of products
Low cost	If scaled up, yes; otherwise, no		When large quantity of products are required, yes; otherwise, moderate
Harsh conditions	Yes, with the enclosed environment		No
R&D pilot studies	Very suitable for the development of new materials and/or material screening		Not suitable, low efficiency and no precise control

and reaction cessation in microreactors is possible. This gives us high uniformity and reproducibility in microreactors. The precise control can also be made automatic when programmable equipment is hooked up to syringe pumps for pressure-driven microreactors. When talking about efficiency, batch-mode reactors can produce a large quantity of products and microreactors seem to lack this advantage due to their small size. However, considering the overall time required for the reaction in both reactors, the productivity in microreactors is comparable to that in batch-mode reactors. Parallel processing can also be used to scale up the production in microreactors, which makes them even more efficient and low cost. For reactions involving expensive materials, the very low consumption of reagents by microreactors makes them stand out compared to batch-mode reactors. With an enclosed environment, microreactors are also suitable for reactions under very harsh conditions. With all these benefits, microreactors are perfect candidates to develop new materials or to screen drugs for research or even industrial purposes.

3. Synthesis of silica materials from microfluidics

Since 2004,[39,40] microfluidics has become an important tool for silica materials synthesis. In this section, we provide a com-

prehensive overview of microfluidics approaches for the synthesis of silica materials. As discussed in the above section, microfluidics synthesis approaches can be broadly divided into two categories: (1) continuous laminar flow synthesis and (2) discrete segment and droplet flow synthesis.

3.1 Continuous laminar flow synthesis

Synthesis of silica materials by continuous laminar flow microreactors is conceptually straightforward. Laminar flow microreactors, in which miscible fluids of reagents are injected into microchannels where they mix and react, are generally simpler in structure and easier to operate. Although relatively fewer research studies to date have focused on the continuous laminar flow synthesis of silica materials, the effort has continued to grow rapidly, especially in the past several years from our group (Table 2). In the following, we will evaluate the capacities of laminar flow microreactors in the synthesis of four main kinds of silica materials: solid spheres, porous spheres, nonspheres, and hierarchical composites.

3.1.1 Solid spheres. Laminar flow synthesis of colloidal solid silica spheres can be as simple as a two-inlet device with one inlet containing a silica precursor (such as tetraethyl orthosilicate, TEOS) and the other a catalyst (such as ammonia) (Fig. 3A).[39] The particle size and its range can be well-controlled by parameters such as linear velocity and mean residence time. For a given laminar flow microreactor design, monodisperse particle distribution is only feasible under the conditions that could minimize axial dispersion. The wider the distribution of residence time, the wider the distribution of particle size.[39,53]

For realizing the high throughput of a microreactor, enhanced fluid mixing at a high flow velocity with a short mixing length is essential. However, conventional microreactors having meander micromixers were always operated at a low flow velocity together with a relatively long mixing microchannel length. To achieve an effective mixing for a wide-range of flow rates in silica nanoparticle synthesis, researchers have developed the planar baffled micromixer (Fig. 3B), which can greatly enhance the mixing performance through the convection-dominant mechanism at high flow rates and the diffusion-dominant mechanism at low flow rates. The sizes of solid silica spheres decreased with increasing flow rate and reaction temperature.[45]

Table 2 Silica materials synthesized from continuous laminar flow microreactors

Microchannel type	Material type	Material size	Material shape	Porous type	Bioapplication area	Ref. by year
Winding	SiO_2	164–321 nm	Sphere	Solid	N/A	2004[39]
Y junction	SiO_2	362–825 nm	Sphere	Solid	GOD immobilization	2008[41]
Coflow	Fe_2O_3@SiO_2	50 nm	Sphere	Solid	N/A	2009[42]
Y junction	SiO_2	200–400 nm	Sphere	Mesopore (~2 nm)	N/A	2010[43]
Slit interdigital	SiO_2	50–300 nm	Sphere	Solid	N/A	2011[44]
Cross junction-baffled mixer	SiO_2	46–250 nm	Sphere	Solid	N/A	2011[45]
Y junction	SiO_2	53–176 nm	Sphere	Solid	N/A	2011[46]
Slit interdigital	SiO_2@Au	~80 nm	Sphere	Solid	N/A	2012[47]
Winding-Spiral	Fe_2O_3@SiO_2@Pt	85 nm	Sphere	Solid	IBA oxidation	2012[48]
Y junction	SiO_2@Au/Fe_2O_3	~200 nm	Sphere	Solid	N/A	2013[49]
Central collision	SiO_2@Au	~100 nm	Sphere	Solid	N/A	2015[50]
Y junction	SiO_2–TiO_2	33 nm	Sphere	Solid	N/A	2015[51]
Slit interdigital and T junction	SiO_2	50–650 nm	Sphere	Hollow; mesopore (~3–4 nm)	N/A	2015[52]
T-shaped	SiO_2; Co_3O_4@SiO_2	~150–650 nm	Sphere	Solid	N/A	2017[53]
Spiral	SiO_2	80 × 150 nm	Ellipsoid	Hollow; mesopore (~3 nm)	Dox drug loading	2017[54]
Flow-focusing	SiO_2	30–80 nm	Sphere	Hollow	N/A	2017[55]
Spiral	SiO_2; SiO_2–QDs/Fe_3O_4	~800 nm	Sphere	Hollow	Cell imaging; RB adsorption; Dox drug loading	2017[56]
Spiral	SiO_2; SiO_2–Ag/Fe_3O_4	~130 × 1500 nm	Fiber	Mesopore (~3 nm)	Dox drug loading; 4-NP reduction	2018[57]
Spiral	SiO_2; SiO_2–FeCo	~2 μm	Flower	Solid	CTC screening	2018[58]
Spiral	Fe_2O_3@SiO_2	~50–350 nm	Sphere; cube; rod; belt	Solid	CTC screening	2018[59]
Spiral	SiO_2	100 nm × 15 μm	Sheet	Hollow; mesopore	RB, BSA, and Dox adsorption	2019[60]
Spiral	Ag@SiO_2	80 × 10 nm	Triangle	Solid	Cellular internalization	2019[61]
Spiral	SiO_2	1.2 μm	Sphere	Hollow; mesopore-macropore (2–100 nm)	4-NP reduction; BSA protein delivery	2019[62]

Abbreviations: 4-NP: 4-nitrophenol; BSA: bovine serum albumin; CTC: circulating tumor cell; Dox: doxorubicin; GOD: glucose oxidase; IBA: 4-isopropyl benzaldehyde; N/A: not applicable; RB: rhodamine B.

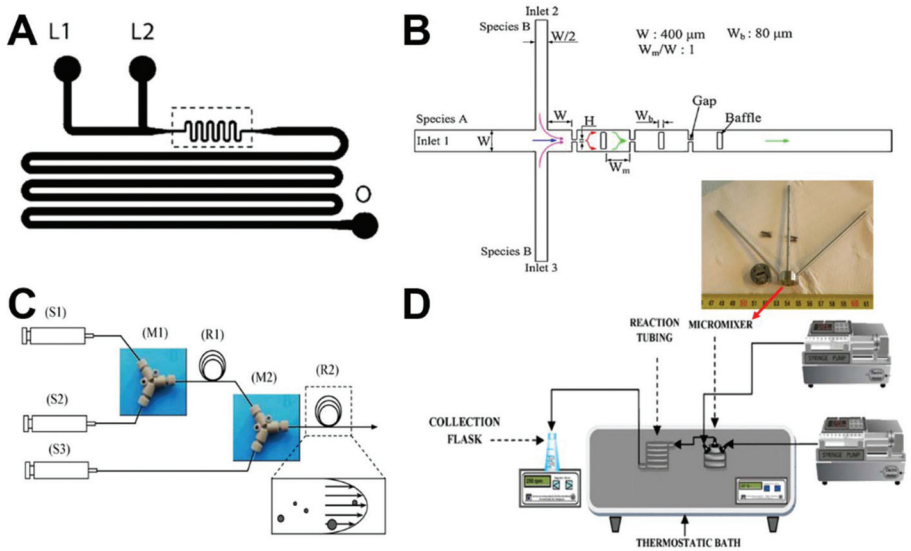

Fig. 3 Examples of laminar flow microreactors for the synthesis of solid silica sphere. (A) Schematic of a microchannel with two liquid inlets (L1 and L2) and one outlet (O). Reproduced with permission from ref. 39. (B) Schematic diagram of the baffled micromixer with three mixing units. Reproduced with permission from ref. 45. (C) Schematic diagram of a microreactor system for silica synthesis. (S1), (S2), and (S3) are syringes for TMOS, HCl, and PEI polymer in Tris-HCl buffer solution, respectively. (M1) and (M2) are Y-shaped mixers. (R1) is the reaction tube for hydrolysis, (R2) is the reaction tube for silica precipitation. Reproduced with permission from ref. 46. (D) Experimental setup using a standard slit interdigital micromixer for the continuous silica particle synthesis. Reproduced with permission from ref. 44.

Compared with batch reactors, microreactors provide fine control over hydrolysis, nucleation, and particle growth. However, for the laminar flow synthesis of silica, deposition of particles on the microchannel walls is almost inevitable, leading to various degrees of clogging and unstable reaction conditions. With the aid of commercial ETFE (Ethylene Tetrafluoroethylene) tubes (Fig. 3C), particle deposition could be minimized and constant flow conditions could be maintained.[46] When employing a polyethylenimine polymer as a nucleation catalyst, a significant narrow size distribution of solid silica spheres can be obtained at room temperature from microfluidics reactors compared to batch reactors.[41,46] In addition to ETFE tubes, a commercially available standard slit interdigital microstructured mixer has been also used to prepare solid silica spheres (Fig. 3D).[44] The interdigital micromixer allows the inlet streams to divide into 16 substreams and recombine for maximizing the contact area, leading to shorter nucleation time and higher homogeneity in terms of composition and temperature. These resulted in a lower polydispersity, narrower particle size distributions, and higher inter-run reproducibility, compared with the batch systems.

3.1.2 Porous spheres. Laminar flow synthesis of porous silica spheres can be realized by the aid of surfactants (such as hexadecyltrimethylammonium salts[43,52,56]) or polymers (such as polyacrylic acid[55]). To prepare uniformly sized porous silica spheres, one feasible way is to separate nucleation and growth processes. Specifically, partial hydrolysis of the silica precursor occurs in the microreactor and then the reaction solution containing the as-synthesized nuclei is added into another solution for silica particle growth (Fig. 4A). Compared to the particles obtained by batch reactors using identical starting solutions, the silica sphere products obtained using microreactors achieved narrower size distributions as a result of the separation of nucleation and growth processes.[43]

For the synthesis of hollow porous silica spheres, our research group first demonstrated the feasibility of a spiral-shaped microreactor with one inlet containing the silica precursor and the other containing the surfactant in diluted ammonia (Fig. 4B).[56] Because of the transverse Dean flow effects, the reactants could achieve instantly complete mixing and hollow silica spheres could be obtained in less than one second. Relying on the hydrodynamic focusing micromixer, hollow silica spheres can also be produced in the presence of poly(acrylic acid) as a template (Fig. 4C). When altering the mixing time by varying the flow rates, small-sized uniform hollow nanospheres can be obtained.[55]

3.1.3 Nonspheres. Compared with spherical counterparts, nonspherical materials have been demonstrated, from both theoretical and experimental perspectives, to possess more advanced biological behaviors, such as higher cellular binding efficiency, better drug/protein loading capacity, larger transmembrane internalization rates, and longer circulation time.[10,63–74] Despite great demand for their synthesis, controllable synthesis of nonspherical silica materials remains a significant challenge. Our research group first opened up this area using spiral-shaped microreactors with two-inlet flows and fabricated a series of nonspherical silica materials, including hollow ellipsoids,[54] fibers,[57] flowers,[58] sheets,[60] and triangles.[61]

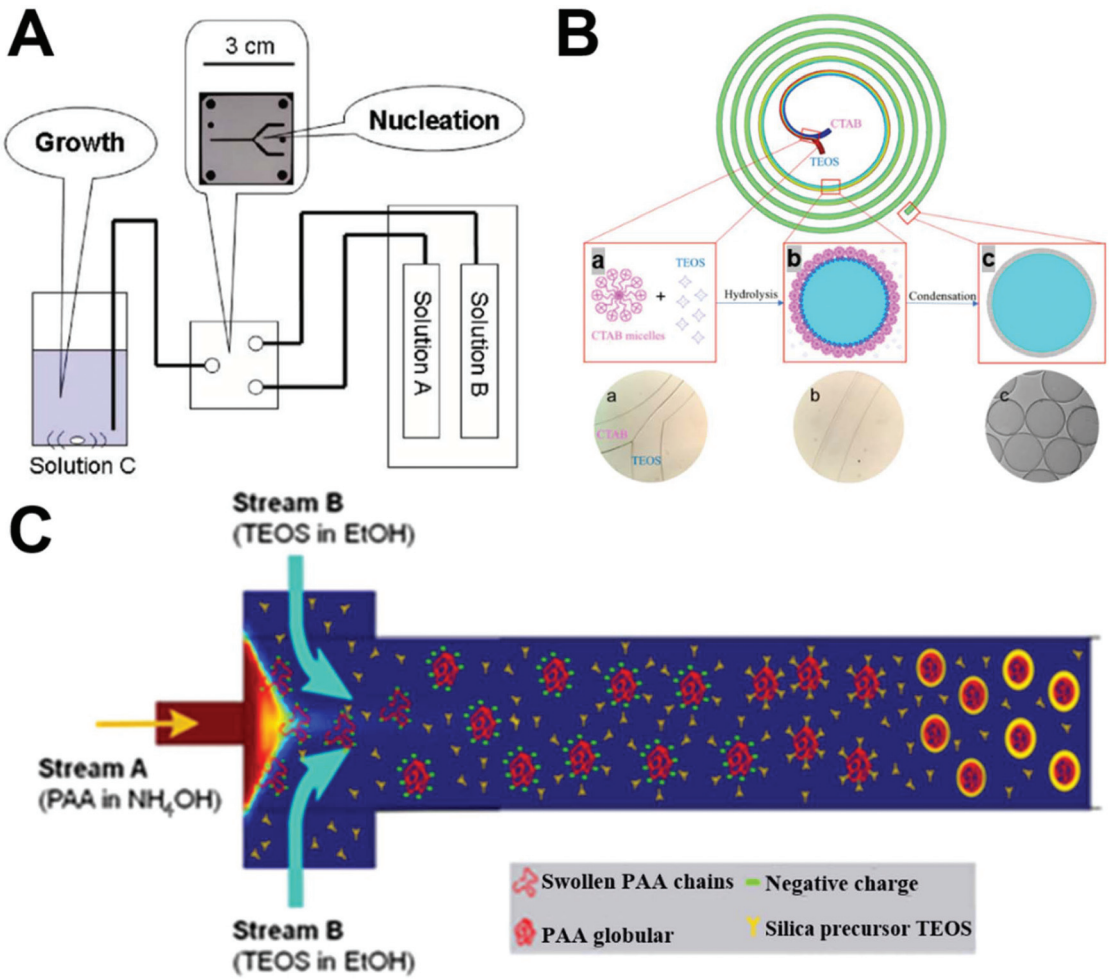

Fig. 4 Examples of laminar flow microreactors for the synthesis of porous silica spheres. (A) Schematic of the reaction setup for the synthesis of nanoporous silica spheres. Solutions A, B, and C are TEOS/MeOH, MeOH aqueous, and CTAC/MeOH aqueous, respectively. Reproduced with permission from ref. 43. (B) Synthesis of submicrometer hollow silica spheres in a spiral-shaped microreactor. (a) TEOS in pure ethanol and CTAB micelles in diluted ammonia were flowed into the spiral microchannel; (b) hydrolysis of TEOS occurred at the interface of the two laminar flows; and (c) hollow silica spheres were collected at the outlet. Reproduced with permission from ref. 56. (C) Formation mechanism of PAA spherical templates in the microreactor with a hydrodynamic focusing micromixer for the synthesis of hollow silica nanoparticles. The mixing profile of the solutions was computed from a COMSOL model. Reproduced with permission from ref. 55.

Microfluidics synthesis of anisotropic hollow ellipsoidal mesoporous silica nanomaterials was realized by a self-templating method. The as-synthesized ellipsoidal mesoporous silica was mixed with bovine serum albumin protein (surface protective coating agent) as one inlet flow, and phosphate buffered saline (etching agent) was used as the other (Fig. 5A). Owing to the rapid and intensive mixing performance of microfluidics, the hollow counterparts can be produced within just several seconds. Comparatively, the batch reactor should need nearly one day.[54] Using the templating methods, the microreactor can be employed as a general and straightforward platform for the synthesis of hollow cubes, hollow rods, hollow belts, and other anisotropic hollow silica materials.[59]

By choosing specific reactants as inlet fluids, we found that nonspherical silica materials can be collected directly from the outlet at certain flow rates. When using cetyltrimethylammonium bromide (CTAB) and diluted ammonia as one inlet flow and diluted tetraethyl orthosilicate (TEOS) as the other, mesoporous silica fibers can be produced (Fig. 5B). The aspect ratios and diameters of silica fibers can be easily tuned by changing the flow rates or the concentrations of reactants.[57] When one inlet flow contains polyvinylpyrrolidone (PVP) and the other has TEOS and hexadecylamine (HDA), silica microflowers with a unique multilayered structure can be obtained at a flow rate as high as 4 mL min^{-1} (Fig. 5C). The production of silica flowers was realized within 94 milliseconds and a yield of nearly 5 grams per hour was achieved.[58] In addition to a five-run spiral-shaped microreactor, we also demonstrated the feasibility of a short-range two-run spiral-shaped microreactor (with a microchannel length of less than 8 cm) for the synthesis of nonspherical silica materials. By choosing CTAB

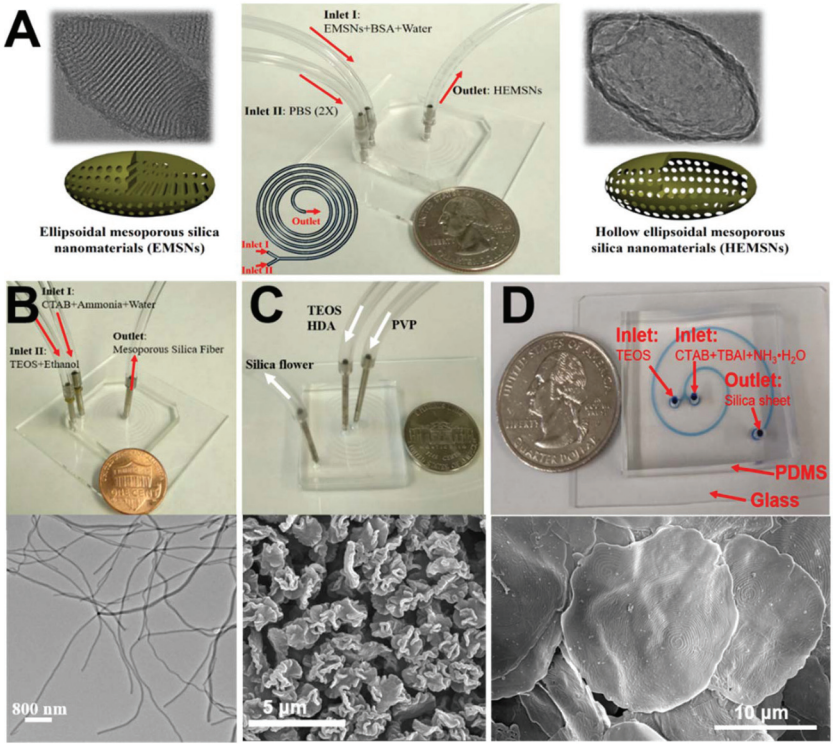

Fig. 5 Examples of laminar flow microreactors for the synthesis of nonspherical silica, including anisotropic hollow ellipsoidal mesoporous silica (A), mesoporous silica nanofiber (B), mesoporous silica microflower (C), and two-dimensional hollow sandwich-like mesoporous silica nanosheet (D). Reproduced with permissions from ref. 54, 57, 58, and 60, respectively.

and tetrabutylammonium iodine (TBAI) as one inlet and TEOS as the other, we successfully fabricated a two-dimensional mesoporous silica nanosheet with a typical hollow sandwich-like bilayer and a unique water-ripple-like wrinkled surface (Fig. 5D).[60]

3.1.4 Hierarchical composites. Silica-based hierarchical composites with two or more tailored physicochemical properties are appealing for a variety of biological applications.[3,75–78] An outstanding advantage of laminar flow microfluidics synthesis systems is that they conveniently allow a combination of individual reactions into a multistep flow sequence. Given this merit, continuous production of hierarchical nanostructures with fluorescent, magnetic, plasmonic and other properties becomes feasible.

Using three tandem coaxial microreactors for the purposes of grafting, mixing, and coating sequentially, the practicability of the multistep synthesis of hierarchical magnetic and fluorescent core–shell Fe_2O_3–SiO_2 was first demonstrated (Fig. 6A).[42] Similarly, nanoparticles with multifunctional (fluorescent, plasmonic, and superparamagnetic) architectures were self-assembled under a continuous flow (SiO_2–Au–Fe_2O_3, Fig. 6B).[49] Besides the simplicity of the microfluidics assembly process and the reproducibility of the as-synthesized products, the time taken for the microsynthesis approach was significantly reduced from several hours for the bulk synthesis to a few minutes.[42,49]

Based on the simple and scalable merits of microfluidics, laminar flow microreactors have attracted considerable attention for the synthesis of many other hierarchical nanocomposites in the past several years. Considering that self-nucleation in the bulk solution phase is suppressed in the microreaction system, no washing is needed after each step. This enables the coupling of seeding and shell growth into a sequential flow in microreactors to synthesize core–shell SiO_2–Au nanocomposites using a commercial slit interdigital microstructured mixer (Fig. 6C) or central collision-type microreactor (Fig. 6D).[47,50] A similar multistep nucleation-controlled growth method can also be employed to synthesize TiO_2–SiO_2 (Fig. 6E),[51] Fe_3O_4–SiO_2–Pt (Fig. 6F),[48] and Co_3O_4–SiO_2 nanocomposites.[53]

Our recent studies first demonstrated the flexibility of two-inlet spiral-shaped microreactors in the synthesis of anisotropic multifunctional hierarchical structures. We found that fluorescent dyes, proteins, quantum dots, magnetic nanoparticles, and/or silver nanoparticles could be simultaneously and efficiently assembled into hollow silica spheres,[56] silica fibers,[57] and silica flower materials.[58] In addition, after fabricating sphere-, cube-, rod-, and belt-shaped magnetic nanoparticles through a spiral-shaped microreactor, we further successfully coated a silica layer on the magnetic particle surface to synthesize differently shaped core–shell Fe_2O_3–SiO_2 nanocomposites. The shell thickness could be well tuned by changing the flow rate of the TEOS fluid.[59]

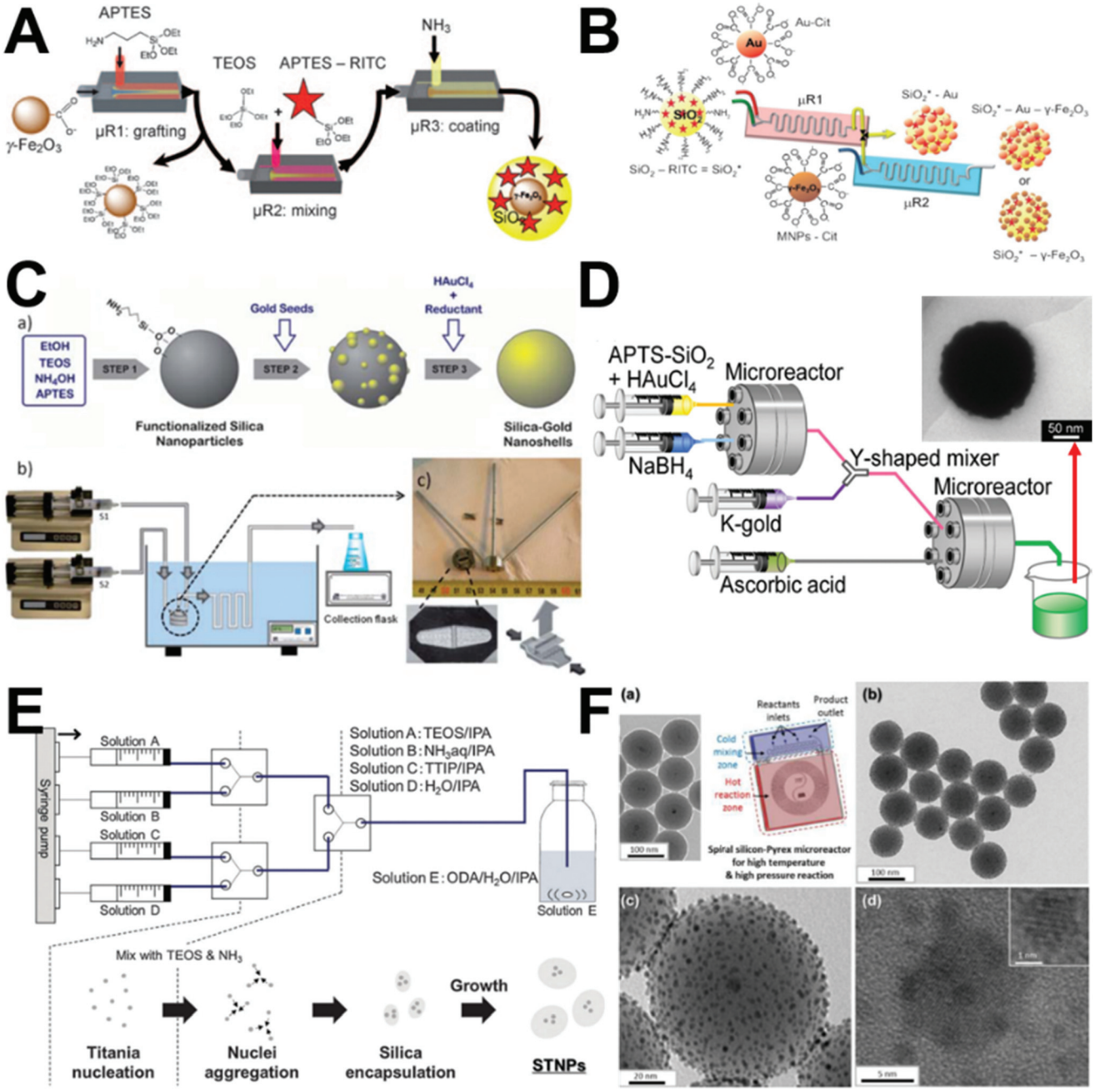

Fig. 6 Examples of laminar flow microreactors for the synthesis of hierarchical composites. (A) Scheme for the continuous synthesis of fluorescent core/shell MNP/silica nanoparticles. Reproduced with permission from ref. 42. (B) A two-step microfluidics synthetic procedure for the assembly of multifunctional nanoparticles/fluorescent silica sphere assemblies. RITC: rhodamine isothiocyanate, Cit: citrate. Reproduced with permission from ref. 49. (C) Experimental process and set-up for the continuous synthesis of SiO_2–Au nanoshells. Reproduced with permission from ref. 47. (D) Sequential flow synthesis of gold-coated silica particles in the central collision-type microreactor. Reproduced with permission from ref. 50. (E) Controlled growth of silica–titania hybrid functional nanoparticles through a multistep microfluidics approach. Reproduced with permission from ref. 51. (F) Synthesis of platinum-decorated magnetic silica nanoparticles in a microfluidics system. Reproduced with permission from ref. 48.

3.2 Discrete segment and droplet flow synthesis

Laminar flow microreactors generally appear to be easier to operate the continuous streams of miscible fluids and under more representative of bulk reaction conditions with improved homogeneity. However, fouling and clogging are unavoidable in most of the continuous flow reactors. Comparatively, discrete segment and droplet flow microreactors, wherein an immiscible gas/liquid is injected alongside the reaction mixture, could attenuate these issues to some extent.[36,37,79,80] Therefore, discrete flow microreactors, especially droplet flow microreactors, have attracted more attention for the synthesis

Table 3 Silica materials synthesized from discrete segment and droplet microreactors

Microchannel type	Material type	Material size	Material shape	Porous type	Bioapplication area	Ref. by year
Winding	SiO_2	277–540 nm	Sphere	Solid	N/A	2004[39]
Winding	SiO_2	200–300 nm	Sphere	Solid	N/A	2004[40]
Winding	SiO_2@TiO_2	~250 nm	Sphere	Solid	N/A	2007[81]
Cross-winding	SiO_2	~15–35 μm	Sphere	Mesopore (>5 nm)	N/A	2008[82]
T junction	SiO_2	0.25–0.5 mm (sphere); 1.1 × 2.3–4.7 mm (rod)	Sphere; rod	Solid	N/A	2008[83]
Cross junction	SiO_2	~1 μm	Sphere	Mesopore (6.4 nm)	N/A	2008[84]
T junction	SiO_2	~100 μm	Sphere	Hollow	N/A	2009[85]
Coflow and flow-focusing	SiO_2	~50 μm	Nonsphere polygon	Hollow	N/A	2009[86]
Cross junction	SiO_2	130 μm	Sphere	Hollow; mesopore (2 nm)	Iodine adsorption	2010[87]
Cross junction	SiO_2–chitosan	250 μm	Sphere	Macropore	BSA immobilization	2010[88]
Coflow-winding	SiO_2	1–5 μm	Sphere	Mesopore (4.8 nm)	N/A	2010[89]
Coflow-winding	SiO_2	1–15 μm	Sphere	Mesopore (4.8 nm)	N/A	2010[90]
Flow-focusing	QDs@SiO_2	~5 μm	Sphere	Hollow	Ultrasound image; lysozyme immobilization	2010[91]
Coflow and flow-focusing	SiO_2	29 μm	Sphere	Hollow	N/A	2010[92]
T junction-winding	SiO_2@Au	177–260 nm	Sphere	Solid	N/A	2010[93]
Y junction-cross junction	SiO_2	63 nm	Sphere	Solid	N/A	2011[46]
Flow-focusing	SiO_2	7–50 μm	Doughnut	Solid	N/A	2011[94]
Coflow	Chitosan@TS-1	200–600 μm	Sphere	Macropore	N/A	2011[95]
Coflow	SiO_2–ETPTA@Ag	77 μm	Sphere	Solid	BT SERS detection	2011[96]
Coflow	SiO_2	100–200 μm	Sphere	Hollow; mesopore (2–38 nm)	N/A	2011[97]
Coflow	SiO_2@TiO_2	100–300 μm	Sphere	Solid	N/A	2011[98]
Coflow	Fe_2O_3@SiO_2@Pt	100 μm	Sphere	Mesopore (18 nm)	IBA oxidation	2012[48]
Flow-focusing	SiO_2–FITC	50–350 nm	Sphere	Solid	N/A	2012[99]
Flow-focusing	SiO_2	1.4–14.6 μm	Sphere	Hollow; mesopore (7.44 nm)	N/A	2012[100]
Coflow	SiO_2–HDDA	~0.5 μm	Patchy	Mesopore	N/A	2012[101]
Cross junction	SiO_2	7.7 μm	Sphere	Mesopore (3.4–6 nm)	N/A	2013[102]
Flow-focusing	SiO_2–lipid	~25 μm	Sphere	Mesopore (13.4 nm)	FFB, FSM, MTX, and RTD drug loading	2013[103]
Coflow	SiO_2–chitosan	420 μm	Sphere	Mesopore (<5 nm)	Cu(II) adsorption	2013[104]
Coflow	SiO_2–Fe_3O_4	150 μm	Sphere	Mesopore	Optical encoding	2013[105]
T junction	SiO_2@Au	230 nm	Sphere	Solid	N/A	2013[106]
T junction	SiO_2	~100 μm	Raspberry-like	Solid	N/A	2013[107]
T junction	SiO_2	90–185 μm	Sphere; filbert-like	Solid; hollow	N/A	2014[108]
Coflow and flow-focusing	SiO_2	~200 μm	Sphere; disk	Mesopore	N/A	2014[109]
Coflow	SiO_2–PEGDA	~200–1000 μm	Rod; cuboid; disk	Solid	Optical encoding	2014[110]
Coflow and flow-focusing	SiO_2–dextran	150–400 nm	Sphere	Mesopore	PTX, SFN, and MTX drug loading	2015[111]
T junction	SiO_2@Fe_2O_3	~100 nm	Sphere	Solid	N/A	2015[112]
T junction	SiO_2@Au	~175 nm	Sphere	Solid	N/A	2015[113]
Coflow and flow-focusing	SiO_2–PEGDA	~100–150 nm (diameter)	Fiber	Macropore	N/A	2016[114]
Y junction and T junction	SiO_2–cell	1.3–2.9 mm	Sphere	Solid	*E. coli* encapsulation	2016[115]
T junction	SiO_2; Au@SiO_2	~100–350 nm	Sphere	Solid (Au@SiO_2); mesopore (SiO_2)	N/A	2016[116]
Slit interdigital	SiO_2–FITC	10–65 nm	Sphere	Solid	N/A	2017[117]
T junction	SiO_2–Fe_3O_4	260 μm	Sphere	Mesopore	OTA adsorption	2017[118]
Flow-focusing	SiO_2	~10–30 μm	Sphere	Hollow; mesopore (5.9 nm)	N/A	2017[119]
T junction	SiO_2	187 μm	Sphere	Mesopore–macropore	DEX drug loading	2018[120]

Table 3 *(Contd.)*

Microchannel type	Material type	Material size	Material shape	Porous type	Bioapplication area	Ref. by year
Cross junction	SiO_2–PCL	~50 μm	Sphere	Solid; macropore	SOD and CAT immobilization	2018[121]
Coflow	SiO_2–PLGA	~200 μm	Sphere	Hollow; mesopore	DFO drug loading	2018[122]
Cross junction	PDT@SiO_2	~90 μm	Sphere	Solid	N/A	2018[123]

Abbreviations: BSA: bovine serum albumin; BT: benzenethiol; CAT: chloramphenicol acetyltransferase; DEX: dexamethasone; DFO: deferoxamine; ETPTA: ethoxylated trimethylolpropane triacrylate; FFB: fenofibrate; FITC: fluorescein isothiocyanate; FSM: furosemide; HDDA: 1,6-hexanediol diacrylate; IBA: 4-isopropyl benzaldehyde; MTX: methotrexate; N/A: not applicable; OTA: Ochratoxin A; PCL: polycaprolactone; PDT: poly(1,10-decanediol dimethacrylate-*co*-trimethoxysillyl propyl methacrylate); PEGDA: poly(ethylene glycol) diacrylate; PLGA: poly(lactic-*co*-glycolic acid); PTX: paclitaxel; QDs: quantum dots; RTD: ranitidine; SERS: surface-enhanced Raman scattering; SFN: sorafenib; SOD: superoxide dismutase; TS-1: titanium silicate molecular sieves.

of silica materials since their discovery (Table 3). In the following, we will discuss in detail about the synthesis of solid spheres, porous spheres, nonspheres, and hierarchical composite silica materials in segment and droplet flow microreactors.

3.2.1 Solid spheres. Segment gas–liquid flow microreactors could eliminate axial dispersion effects and thus yield silica spheres of better quality than laminar flow microreactors.[39,46] Through quantifying the recirculation motion in liquid segments and the symmetric characteristics of the recirculations associated with gas–liquid flows, it was found that the geometries of segment microreactors significantly affect the mixing performance. Even minor surface roughness property and the compressibility of the gas phase could induce loss of symmetry and enhance the mixing across the centerline of the straight microchannel, while mixing could be further accelerated in the meandering microchannel by the periodic switching of recirculation patterns across the microchannel center (Fig. 7A).[40] This phenomenon confers a narrowed liquid-phase residence time distribution in segmented flows, where narrow particle size distributions of solid silica spheres could be obtained compared with the laminar flow counterparts.[39,40,46]

Droplet-based microreactors for the synthesis of solid silica spheres are implemented by a continuous aqueous phase and a dispersed oil phase, which can be FC-40 fluorinert oil (Fig. 7B),[99] silicone oil,[83] liquid paraffin (Fig. 7C),[108] cyclohexane and 1-hexanol (Fig. 7D).[117] Due to precise control of reagent concentrations and residence time, synthesis in droplets could lead to a faster reaction and provide drastically improved silica nanosphere size uniformity compared with conventional bulk synthesis methods.[99] By varying the flow rates of continuous and dispersed phases, sizes of solid silica spheres from droplet flow microreactors can be controlled, and even hundreds of micrometer- or millimeter-scale silica particles can be continuously produced,[83] which is generally hard to achieve from laminar flow microreactors. A droplet microreactor can be also employed to assist the formation of solid silica microspheres by immersing the formed monodisperse silica sol droplets into the extractant solvent fatty acid methyl ester at room temperature (Fig. 7C).[108] In addition, combining an emulsion technique and interdigital mixers, droplet microreactors could achieve high throughput production with a high reproducibility (Fig. 7D).[117]

3.2.2 Porous spheres. Discrete microreactors for the synthesis of porous silica spheres are generally driven by the assembly of nanosized silica particles to form products around tens of micrometers in diameter. Most studies in this area reported to date have been carried out on droplet-based microreactors; research methods on segment flow microreactors are very few. The gas–liquid interface formation of hollow porous silica spheres can be realized by local perturbations of pH on the length scale of an individual bubble. Specifically, after the generation of monodisperse gas bubbles in an aqueous dispersion of anionic silica nanoparticles, the rapid dissolution of gas could result in the shrinkage of bubbles and increase the acidity of the solution in the neighborhood of the bubbles. This leads to the adsorption of silica nanoparticles at the gas–liquid interface driven by the chemically induced *in situ* change in the surface energy of the particles (Fig. 8A). This method enables the single-step production of silica armored bubbles with narrow polydispersity (below 5%) and high producibility (up to 3000 bubbles per second).[85]

For droplet flow microreactors, many studies relied on the solvent evaporation or solvent diffusion methods for the self-assembly formation of porous silica spheres. Microfluidics diffusion-induced self-assembly, which combines microfluidics generation of uniform droplets and subsequent *in situ* rapid solvent diffusion-induced self-assembly inside the microchannel, can be easily implemented for the synthesis of monodisperse porous silica microspheres.[82,120] The particle size can be controlled by simply adjusting the microfluidics conditions such as flow focusing geometry and relative flow rates of two immiscible solutions (Fig. 8B).[82] Similarly, hollow porous silica spheres can be generated in a capillary microfluidics device using either an air-in-oil-in-water bubble templating assembly method (Fig. 8C) or a double emulsion templating assembly method (Fig. 8D). Upon the evaporation of the organic solvent, the silica nanoparticles in the oil layer form a stiff shell at the interface and yield porous silica microspheres.[92,97]

In addition to the self-assembly method, porous silica microspheres can be generated using optimized droplet-based

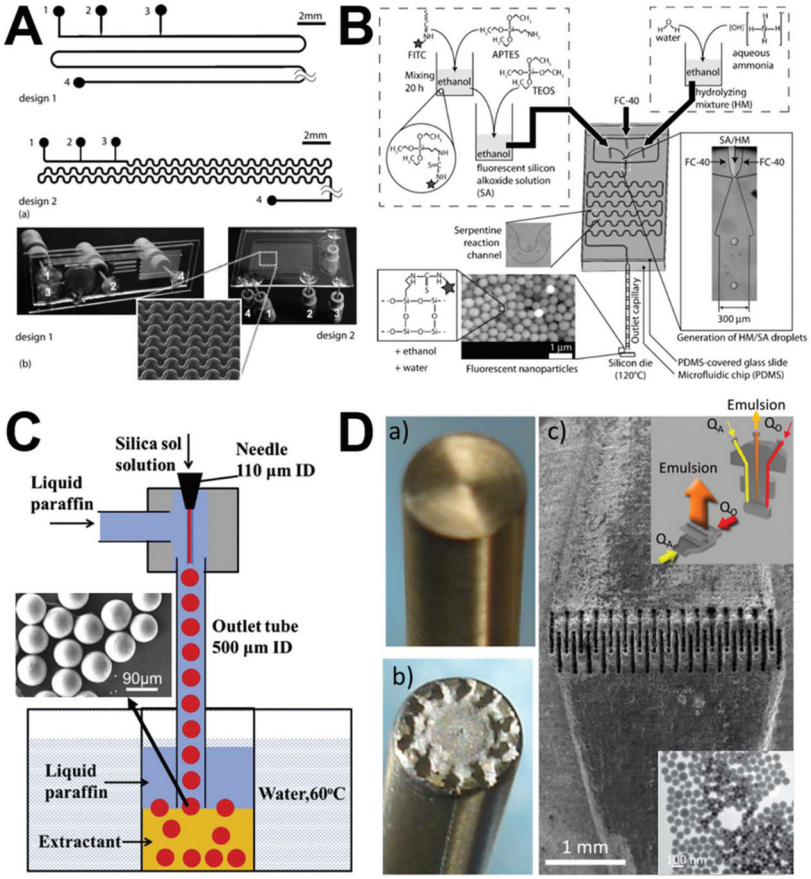

Fig. 7 Examples of discrete segment and droplet microreactors for the synthesis of solid silica spheres. (A) Segmented gas–liquid flow microreactors with straight-walled channels (design 1) and meandering channels (design 2) for solid silica sphere synthesis. Number 2 is the gas inlet. Reproduced with permission from ref. 40. (B) Procedure and setup for the droplet-based synthesis of silica spheres. Reproduced with permission from ref. 99. (C) Droplet synthesis of silica microspheres. Reproduced with permission from ref. 108. (D) A microfluidic interdigital mixer used to produce silica nanospheres by microchannel emulsification. Reproduced with permission from ref. 117.

sol–gel methods. For example, the sol–gel reaction can be activated by coalescing droplet pairs and fast mixing inside the coalesced droplets using a double step-emulsification device (Fig. 8E), and the size can be easily tuned by varying the flow rates, the dimensions of the microfluidics device, and the chemical concentrations.[89,90] By templating silica microparticles with a specially designed surfactant micelle/oil nanoemulsion mixture, silica spheres with hierarchical porosity can be formed; the size distribution and surface area of the smaller micelle-templated pores are controlled as a sequence of altering the hydrophobic chain length of the molecular surfactant templates.[84,102] Similarly, hollow porous silica microspheres with controllable size can be produced *via* hydrolysis and polymerization of the silica precursor at the interface of water-in-oil droplets by a microfluidics-assisted sol–gel process (Fig. 8F).[87,100,108,119]

3.2.3 Nonspheres. In droplet formation of nonspherical silica, the ability to control the local flow field *via* the fabrication of complex microscale geometries enables control over the deformation or breakup of every individual droplet, thus allowing control over particle morphology. By placing the microchannel vertically, the droplets can adopt a rod shape because the confinement suppresses the relaxation of their shape to the spherical equilibrium one. Aspect ratios of the rod-like droplets can be easily controlled by changing the ratio of the droplet volume to the diameter of the cylindrical microchannel (Fig. 9A).[83] Nonspherical silica colloidosomes with multiple compartments can be obtained using a glass capillary microfluidics system that combines a co-flow and a flow-focusing geometry to prepare W/O/W double emulsions (Fig. 9B), where a different number of internal aqueous drops are confined in the oil drop containing hydrophobic silica nanoparticles. During the oil removal, the internal water-in-oil interface retains their spherical shape and the outer oil-in-water deforms, leading to the formation of nonspherical silica with multiple compartments inside.[86] Such solvent evaporation-induced structural deformation can be employed to fabricate a series of other nonspherical silica materials, including doughnut-shape (Fig. 9C),[94] raspberry-shape (Fig. 9D),[107] filbert-shape,[108] and disk-shape.[109] In addition, by photopolymerizing the droplet templates within the confined microchannels, anisotropic silica particles with the same ordered

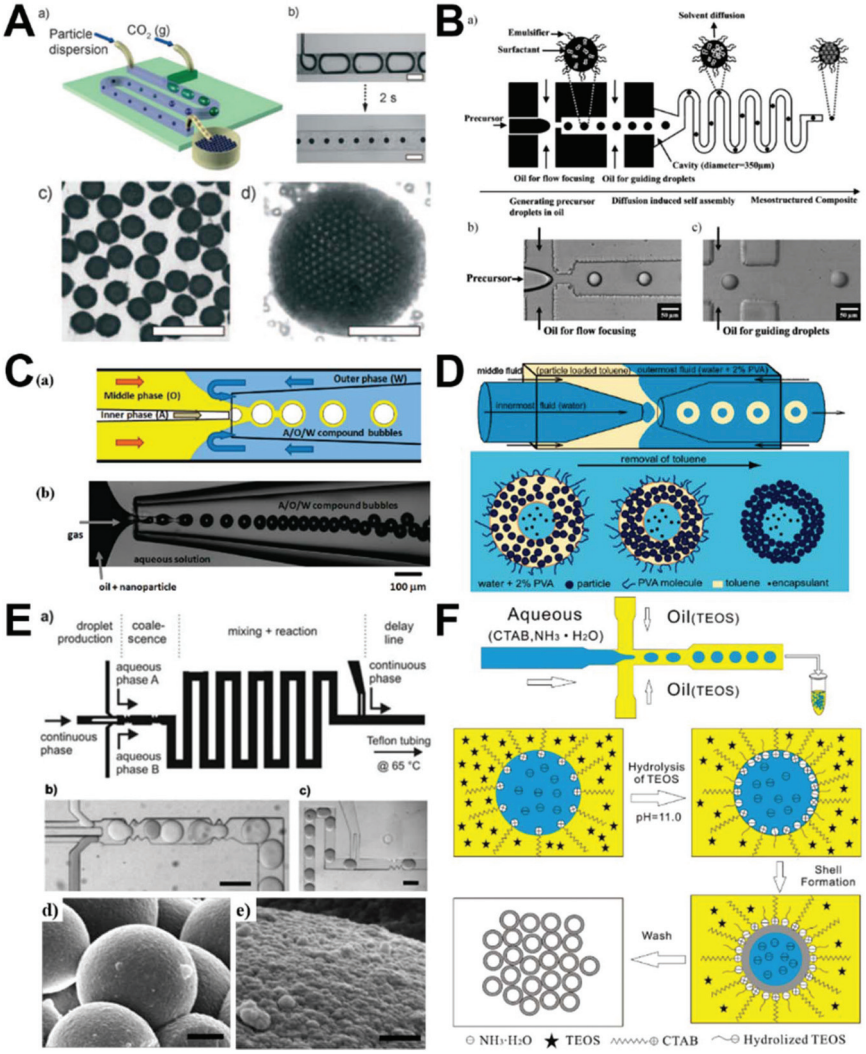

Fig. 8 Examples of discrete segment and droplet microreactors for the synthesis of porous silica spheres. (A) Microfluidics assembly of armored bubble-like colloidal silica by dissolving CO_2. Reproduced with permission from ref. 85. (B) Generation of monodisperse mesoporous silica microspheres using microfluidics diffusion-induced self-assembly. Reproduced with permission from ref. 82. (C) Microfluidics fabrication of silica nanoparticle-shelled bubbles using air-in-oil-in-water (A/O/W) compound bubbles as templates. Reproduced with permission from ref. 92. (D) Schematic illustration of the double emulsion generation process in a double microcapillary device (top) and the formation of colloidosomes by solvent removal (bottom). Reproduced with permission from ref. 97. (E) Template-free preparation of mesoporous silica spheres through a double step-emulsification microfluidics device. Reproduced with permission from ref. 90. (F) Schematic illustration of the droplet microfluidics approach for preparing monodisperse hollow silica microspheres through interfacial polymerization in water-in-oil droplets. Reproduced with permission from ref. 87.

colloidal structures can be generated,[110] which will be discussed further in the following section.

3.2.4 Hierarchical composites. Discrete flow synthesis of hierarchical composites has been studied extensively compared with other particle synthesis systems mentioned above. There are a variety of silica-based inorganic–inorganic and inorganic–organic core–shell and Janus materials formed through segment and droplet flow microreactors. To date, gas–liquid segment flow microreactors, although there are still relatively few reported studies, have demonstrated their great potential in the controllable synthesis of core–shell silica materials, including SiO_2@TiO_2 (Fig. 10A),[81] SiO_2@Au (Fig. 10B),[93,106] and Au@SiO_2.[116] Since the batch synthesis of core–shell silica materials always suffers from difficulties in controlling overcoat thickness, maintaining a narrow size distribution, and avoiding secondary nucleation and aggregation, segment flow microreactors provide efficient alternative solutions by the distinctive merit of highly flexible designs, such as multi-point addition of a shell reactant (Fig. 10A) and multi-phase inlet motifs (Fig. 10B).

Droplet flow microreactors enable the production of inorganic–inorganic (Fig. 10C & E) and inorganic–organic (Fig. 10D & F) silica composites at the oil–aqueous interface. The formation of most silica-based inorganic–inorganic core–

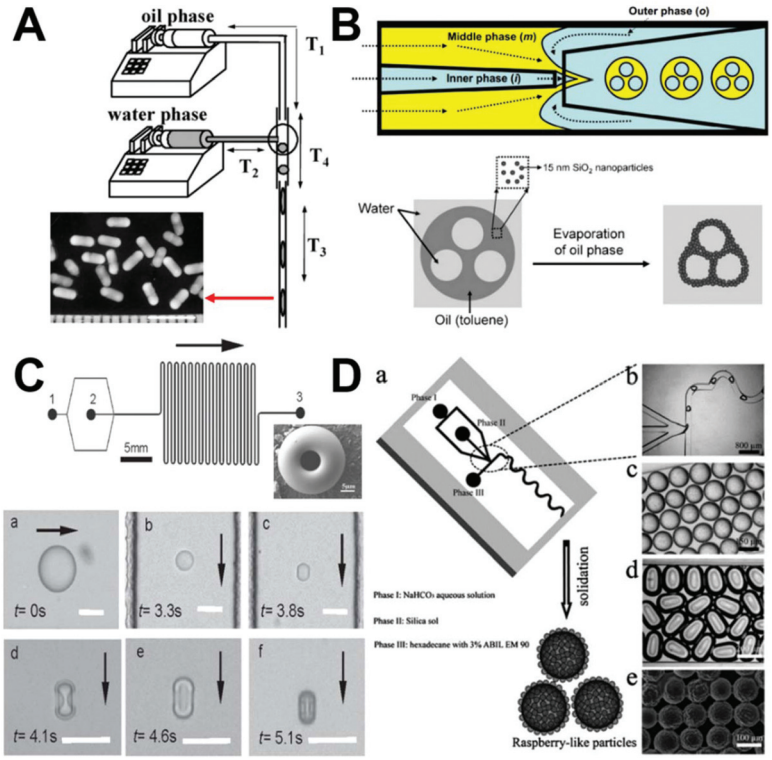

Fig. 9 Examples of discrete segment and droplet microreactors for the synthesis of nonspherical silica. (A) Experimental setup for the synthesis of anisotropic silica rod particles. Reproduced with permission from ref. 83. (B) Generation of nonspherical colloidosomes from W/O/W double emulsions with multiple internal aqueous drops using a glass capillary microfluidics channel. Reproduced with permission from ref. 86. (C) Template-free formation of monodisperse doughnut-shaped silica microparticles by droplet-based microfluidics. Reproduced with permission from ref. 94. (D) Microfluidics synthesis of monodisperse hierarchical silica particles with raspberry-like morphology. Reproduced with permission from ref. 107.

shell and Janus hybrids relies on a microfluidics-assisted self-assembly method. For example, using different geometries of microchannels, silica–magnetic composites can be produced through a one-step emulsion process[105,118] or multistep sequential manipulation process (Fig. 10C);[112] core–shell silica–titania can be obtained using a one-step emulsion process in a co-axial microdevice;[98] Janus silica–gold nanohybrids can be assembled at the interface of microdroplets produced by the emulsification of an aqueous suspension of gold nanoparticles in an organic phase composed of a suspension of silica nanoparticles in cyclohexane (Fig. 10E).[113] Similarly, silica-based inorganic–organic hybrids with controlled structures and desired properties can be fabricated using microfluidics technology owing to its capability for precisely controlling the emulsification process and for generating monodispersed compound droplets inside microchannels. Of these organic components of silica–polymer composites, chitosan is the most favorable one due to its inherent abundant amine groups that are readily capable for heavy metal ions adsorption, protein immobilization, and molecular catalysis.[88,95,104] In addition, for the synthesis of silica–polymer hybrids, chemical crosslinking (such as glutaraldehyde[88,95,104]) and physical crosslinking methods (such as ultraviolet irradiation[96,101,110,114,123]) are always used during the solidification process. However, the former generally can produce only spherical composites (Fig. 10D),[95] while the latter enables the synthesis of anisotropic hierarchical structures, such as fiber,[114] patchy particle,[101] rod, cuboid, and disk (Fig. 10F).[110]

4. Biomedical applications of silica materials from microfluidics

Silica materials synthesized from microfluidics reactors have demonstrated more advanced properties than those from conventional batch reactors, such as uniform size distributions, ease of functionalization, flexible morphology tunability, and facile scale-up. These features make the resultant silica materials derived from microreactors attractive for bioapplications in bioimaging, protein immobilization, bioadsorption, drug delivery, liquid biopsy, *etc*. In the following, we will provide an overview of the application progress of silica biomaterials from continuous and discrete microreactors.

4.1 Bioimaging

Microfluidics provides great opportunities for the synthesis of new silica bioimaging agents by either assembly[91,105,110] or sol–gel chemical reactions.[56] For the synthesis of efficient ultrasound imaging agents, droplet microreactors could easily assemble silica-coated CdSe/ZnS QD nanoparticles on the

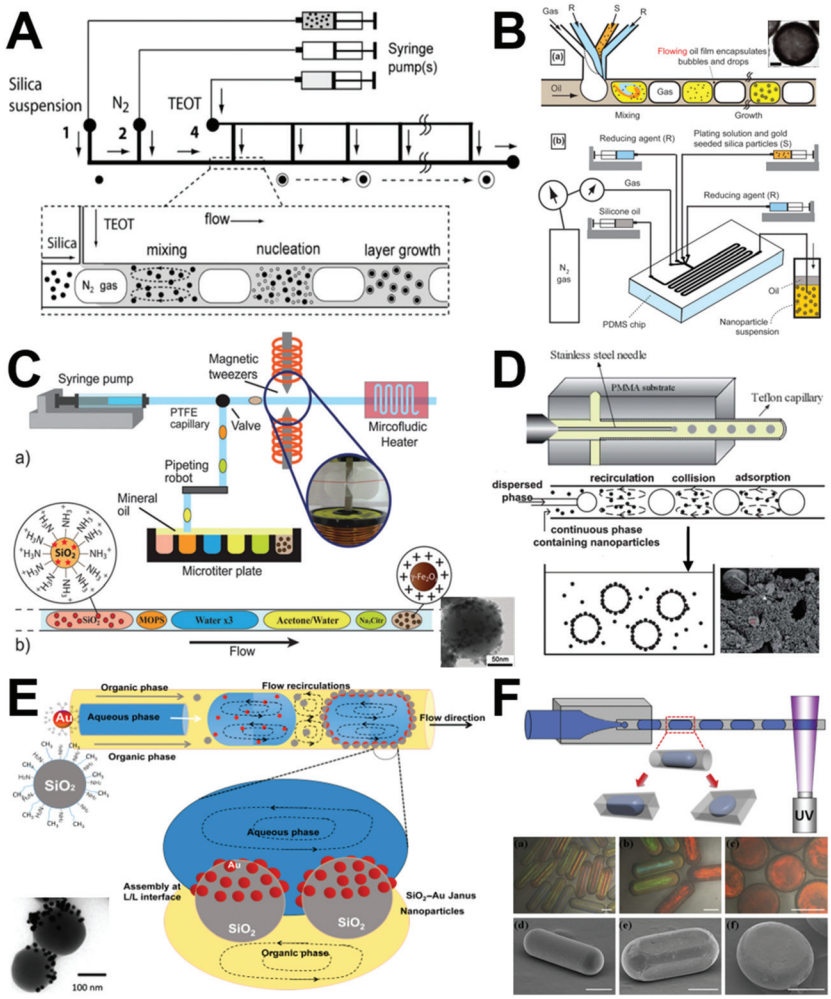

Fig. 10 Examples of discrete segment and droplet microreactors for the synthesis of hierarchical composites. (A) Microfluidics synthesis of titania shells on colloidal silica (SiO_2@TiO_2) at the gas–liquid interface. Reproduced with permission from ref. 81. (B) Microfluidics foam generation of plasmonic nanoshells on a silica surface. Reproduced with permission from ref. 93. (C) Microfluidics droplet flow synthesis of silica nanoparticles coated with iron oxide nanoparticles. Reproduced with permission from ref. 112. (D) Droplet flow synthesis of silica–chitosan hybrid microsphere in a coaxial microfluidics device. Reproduced with permission from ref. 95. (E) Droplet liquid–liquid interfaces generated in a microfluidics device for assembling Janus inorganic nanohybrids (SiO_2–Au). Reproduced with permission from ref. 113. (F) Schematic illustration of the microfluidics device used for the generation of anisotropic particles with various geometries. The resultant droplets were solidified *in situ* using UV irradiation. Reproduced with permission from ref. 110.

surface of perfluorocarbon microbubbles *via* the electrostatic attraction between nanoparticles and the microbubble shell. *In vitro* ultrasound images demonstrated that, compared to microbubbles alone, silica-QD-incorporated microbubbles obviously improved the signal intensity in both contrast-specific imaging and B-mode imaging (Fig. 11A).[91] Based on the self-assembly of droplet microreactors, silica–magnetic Janus and nonspherical photonic crystal particles can also be produced by the emulsification and photo-polymerization process, respectively.[105,110] The distinguishable features of resultant particles make them ideal barcodes for optical encoding. A DNA multiplex coding bioassay showed that these photonic crystal particles have a great encoding capacity and obvious detection signal enhancement within 20 min (Fig. 11B). Using a two-inlet spiral-shaped laminar flow microreactor, our research group developed a facile protocol to synthesize fluorescent silica microspheres by just adding fluorescent dyes, proteins, or QDs into one inlet flow. The as-synthesized fluorescent silica particles can effectively interact with SK-BR-3 cancer cells with negligible cytotoxicity (Fig. 11C).[56] These preliminary results revealed the promising potential of silica bioimaging agents from microreactors. However, further studies are needed to demonstrate their practical applicability in clinical settings.

4.2 Protein immobilization

The immobilization of proteins on microreactor-generated silica materials is feasible by either a microfluidics process (Fig. 12A-a) or a conventional batch process (Fig. 12B-a). A better control of the operation parameters in the microfluidics

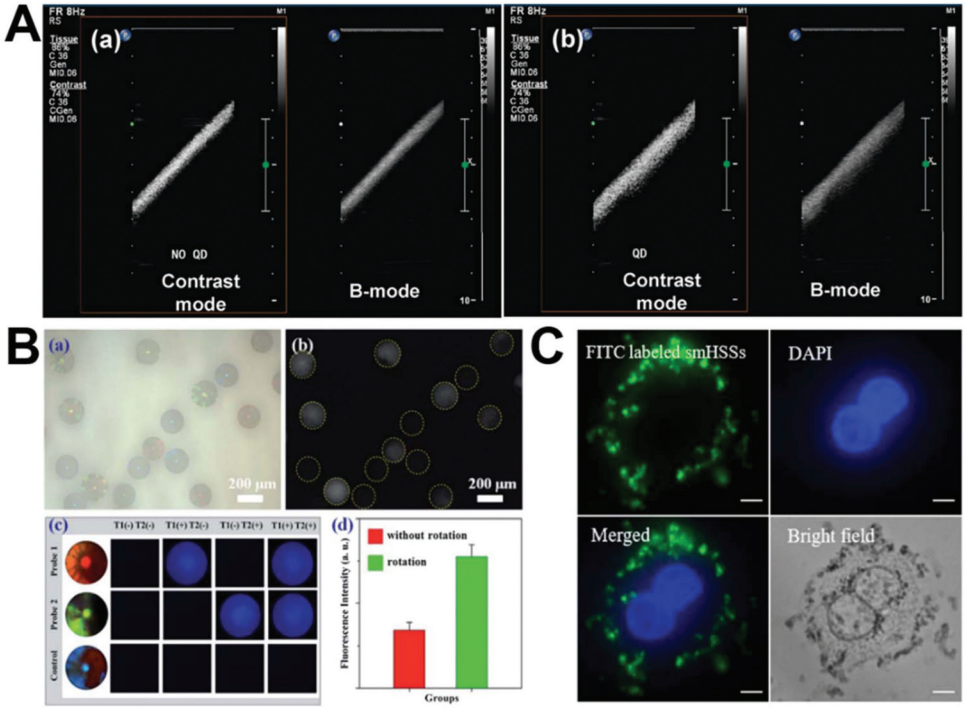

Fig. 11 Microfluidics synthesis of silica-based biomaterials for ultrasound imaging (A), optical encoding (B), and cell imaging (C). (A) *In vitro* ultrasound images of an Opticell filled with unloaded microbubbles (a) and microbubbles loaded with silica-coated QDs. Reproduced with permission from ref. 91. (B) Microfluidics generation of magnetic–silica Janus photonic crystal particles for optical encoding. Reproduced with permission from ref. 105. (C) Fluorescent images of SK-BR-3 cells after incubated with hollow silica spheres for 4 hours. Reproduced with permission from ref. 56.

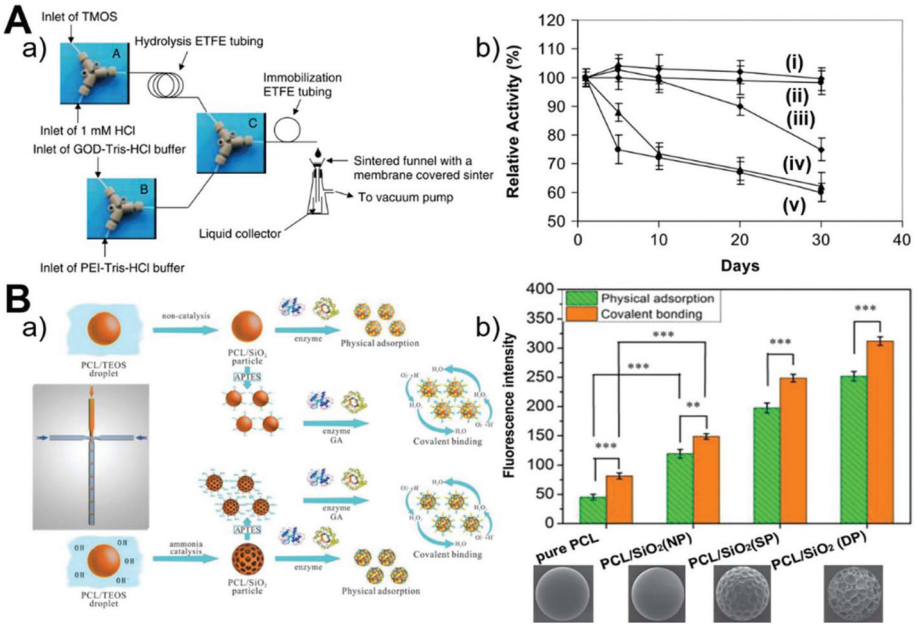

Fig. 12 Microfluidics synthesis of silica-based biomaterials for protein immobilization. (A) Continuous flow microfluidics reactor system used for the immobilization of GOD in silica nanoparticles (a) and the comparison of the stability of immobilized GOD and GOD in solution (b, from i to v are a microreactor system using R5 peptide, microreactor system using PEI, batch reactor system, two-step batch reactor system with silica particle synthesis firstly and then GOD immobilization using PEI, and free GOD in solution, respectively). Reproduced with permission from ref. 41. (B) Microfluidics fabrication of hierarchical PCL–silica hybrid microbeads for multiprotein coimmobilization (a) and the comparison of the fluorescence intensity of cy3–BSA (red) and FITC–IgG (green) immobilized microbeads. NP: no pore; SP: shallow pore; DP: deep pore. Reproduced with permission from ref. 121.

methodology over batch methodology is expected to enable the production of silica particles with optimal structural properties for efficient protein immobilization with long-term stability. A continuous laminar flow microreactor was demonstrated to successfully immobilize glucose oxidase (GOD) in the presence of a polyethylenimine (PEI) polymer or R5 peptide. Microfluidics-immobilized GOD shows no loss of activity over at least a 30-day period; however, batch immobilization causes a significantly reduced activity of GOD after ten days (Fig. 12A-b).[41] Similarly, the droplet flow microreactor allows a one-step process for the immobilization of bovine serum albumin (BSA) protein during the synthesis of chitosan–silica microspheres. The existence of silica in the chitosan spheres can enhance protein loading capacity (up to 50 mg g^{-1}), which further increases with increased silica precursor concentration.[88] In addition to the precise control on the particle size and shape, a droplet-based microreactor also permits adjusting the surface porosity of poly(ε-caprolactone)/silica (PCL/SiO_2) hybrid microbeads for effective protein coimmobilization. In comparison with physical adsorption, covalent binding favors IgG and BSA coimmobilization more remarkably, and the higher degree of surface porosity results in higher loading amounts of proteins (Fig. 12B-b).[121] Although these results revealed the important roles of the immobilization methodology and particulate structure on protein immobilization, the protein loading efficiency on silica materials is still very low and more efforts need to be made to improve the synergistic performance through multiprotein coimmobilization.

4.3 Bioadsorption

For the purpose of ion and molecule adsorption, droplet flow microreactors are generally employed to synthesize a couple of hundred micrometer-sized silica materials with typical porous structure.[87,104,118] The synthesized hollow silica microspheres from droplet flow microreactors offer a much higher storage capacity compared to those from batch reactors, making them suitable for iodine adsorption. The removal rate of iodine of over 95% within 30 seconds after adding hollow microspheres could be achieved (Fig. 13A).[87] Silica-doped porous chitosan/silica hybrid microspheres were also demonstrated to have faster adsorption kinetics and a larger equilibrium adsorption amount of Cu(II) compared to porous chitosan microspheres.[104] In addition to ions, photonic encoding magnetized silica microspheres from a droplet microreactor can be applied to the aptamer-based adsorption of the food toxin Ochratoxin A (OTA) with up to 80% enrichment efficiency (Fig. 13B).[118] Different from the above-mentioned batch process for bioadsorption, our group first investigated the feasibility of the microfluidics process for the on-chip enrichment of biomolecules in a two-run spiral-shaped laminar flow microreac-

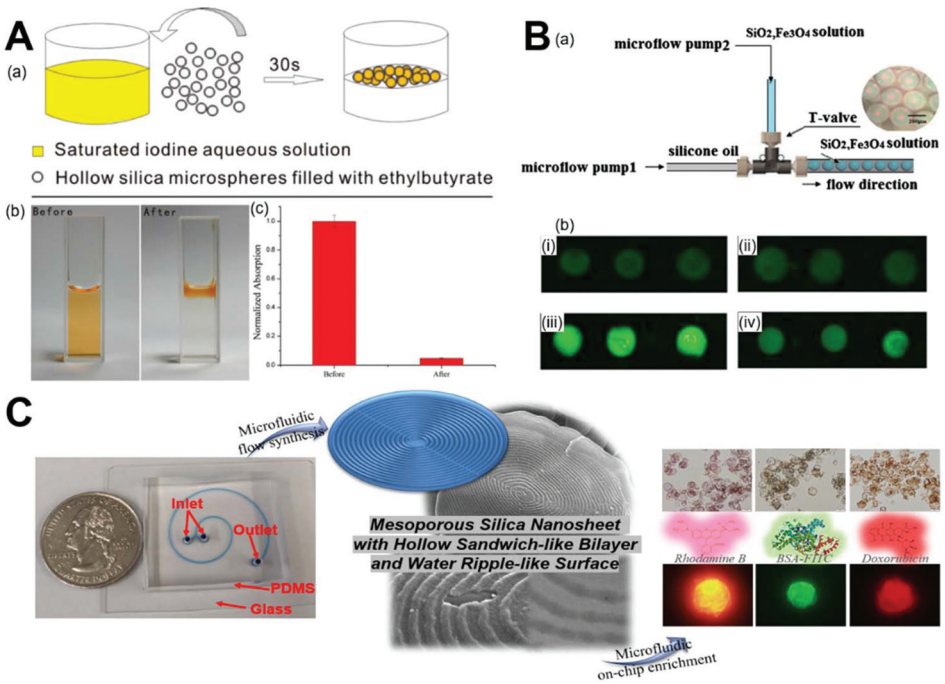

Fig. 13 Microfluidics synthesis of silica-based biomaterials for ion and molecule adsorption. (A) Droplet flow synthesis of hollow silica microspheres for iodine adsorption. Reproduced with permission from ref. 87. (B) Droplet synthesis of porous photonic encoding magnetized silica microspheres (PEMSMs) for OTA enrichment. Figures i–iv are carbonylated surfaces of PEMSMs, physical adsorption of the OTA aptamer on the surface of PEMSMs, covalent bonding of the OTA aptamer on the surface of PEMSMs with NHS/EDC activation, and covalent bonding of the OTA aptamer with a biotin–streptavidin link system on the surface of PEMSMs, respectively. Reproduced with permission from ref. 118. (C) Microfluidics synthesis of a two-dimensional hollow sandwich-like mesoporous silica nanosheet with a water ripple-like surface for on-chip enrichment of rhodamine B, BSA–FITC, and doxorubicin. Reproduced with permission from ref. 60.

tor. The two inlets of a microfluidics device, one containing a mesoporous silica nanosheet as an adsorbent and the other containing rhodamine B, BSA–FITC, or doxorubicin as an adsorbate, were operated at different flow rates for examining the enrichment capacity (Fig. 13C). Both theoretical analysis and experimental tests demonstrated the rapid and efficient on-chip enrichment capacity of the mesoporous silica nanosheet. The lower the flow rate ratio of the adsorbate to the adsorbent, the higher the adsorption rates of silica materials. The maximum on-chip adsorption amounts of rhodamine B, BSA–FITC, and doxorubicin were 1.24, 0.55, and 0.93 gram per gram of silica sheet material, respectively.[60] Compared to the batch adsorption process, the microfluidics process could realize ultrafast on-chip enrichment of ions and molecules at the millisecond time scale; however, the throughput is still a big issue.

4.4 Drug delivery

Compared to the post-synthesis batch loading approach of drugs,[54,56,120] the microfluidics approach permits one-step encapsulation of aqueous insoluble and aqueous soluble drugs during the formation of resultant silica-based biomaterials, which significantly simplifies the drug loading procedures.[111,122] To achieve sustained drug delivery, microfluidics can encapsulate drug-loaded thermally hydrocarbonized porous silicon (THCPSi) microparticles within solid lipid microparticles (SLMs). The lipid coating not only enhances the cytocompatibility, but also leads to at least 1.3 times longer release time than that from THCPSi (Fig. 14A).[103] For simultaneous drug loading during material synthesis, microfluidics technology not only avoids the imposition of large shear and strong oscillation on encapsulated drugs, but also tailors the porous structures of silica materials to alter their surface areas. These unique features endow the silica materials with high-drug loading capacity and controlled drug release at a desired rate. Using a double-emulsion droplet microfluidics system, deferoxamine drug-loaded hierarchically porous silica microparticles as a new composite scaffold successfully promoted neovascularization, collagen deposition, and tissue repair in a rat model of a partial abdominal wall defect (Fig. 14B).[122] In addition to single drug loading, a microfluidics device also permits the simultaneous loading of multiple drugs with different physicochemical properties in a ratiometric control. The release kinetics of all the drug payloads can be well controlled by the decomposition rate of the outer polymer matrix on a porous silica surface (Fig. 14C).[111] Furthermore, most of the microfluidics drug loading systems to date have been established on the basis of droplet flow microreactors. Recently, our group was the first to develop a laminar flow microreactor drug loading system with one inlet flow containing CTAB surfactant and doxorubicin and the other inlet flow containing a silica precursor. The drug molecules can be uniformly distributed into the resultant mesoporous silica fiber materials with an encapsulation efficiency of 12.34%, and pH-dependent sustained drug release profiles were observed over 15 days (Fig. 14D).[57] Microfluidics provides great convenience for simplifying the drug-loading process; however, it is to be noted that there is still much room for increasing the drug-loading efficiency, especially for multidrug codelivery systems.

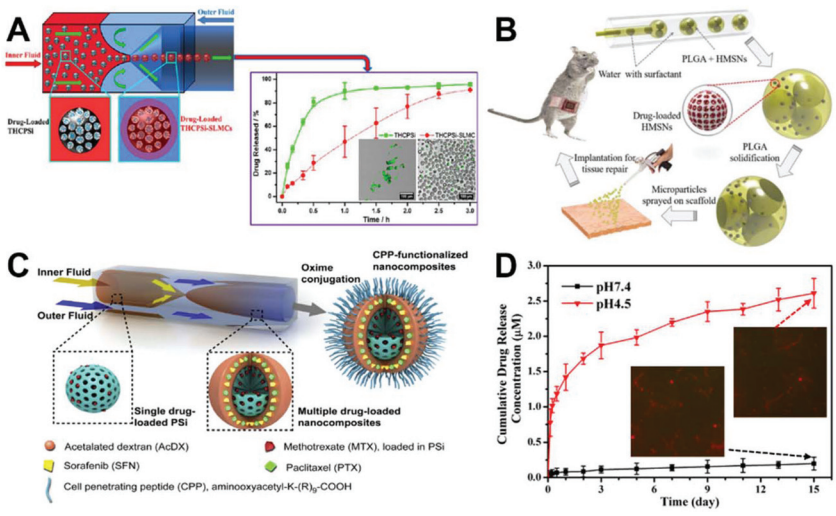

Fig. 14 Microfluidics synthesis of silica-based biomaterials for drug delivery. (A) Microfluidics synthesis of mesoporous silica–solid lipid microcomposite for aqueous insoluble and aqueous soluble drug delivery. Reproduced with permission from ref. 103. (B) Schematic diagram of a capillary microfluidics system for generating W/O/W double emulsion droplets, the fabrication process of the hierarchically porous composite microparticles for controllable drug delivery, and the generation of microparticle-coated scaffold and its application in abdominal wall repair. Reproduced with permission from ref. 122. (C) Schematics of the process to synthesize cell penetrating peptide-functionalized multidrug-loaded PSi@AcDX–CPP. Reproduced with permission from ref. 111. (D) Drug release profiles of microfluidics-enabled one-step production of doxorubicin-loaded mesoporous silica fiber and two representative fluorescent images after drug release tests. Reproduced with permission from ref. 57.

4.5 Liquid biopsy

Compared to conventional tissue biopsies that require a long time to process before analysis and are costly, painful, and difficult to obtain, liquid biopsy represents a new non-invasive approach that has been extensively studied over the past decade and holds great promise.[124] Although great progress in nanomaterial-based circulating tumor biomarker screening has been made, the structure–property–function relationship behind them is still unelucidated. Our research group first employed a microreactor to fabricate differently shaped silica–magnetic immunomaterials and examined the effect of particle shape on the screening performance of circulating tumor cells (CTCs).[58,59] In one recent study, we successfully fabricated sphere-, cube-, rod-, and belt-shaped magnetic nanoparticles and then coated them with a thin silica shell for conjugating epithelial cell adhesion molecule (EpCAM) antibodies and improving their cytobiocompatibility (Fig. 15). The screening results showed that belt-shaped nanoparticles having the largest aspect ratio exhibited the highest capture rates in MCF-7 and MDA-MB-231 tumor cells-spiked whole blood samples, followed by rod-shaped nanoparticles; sphere- and cube-shaped nanoparticles had the relatively lowest capture efficiencies.[59] In another study, we created silica–magnetic microflowers with unique multilayered structures in a spiral-shaped laminar flow microreactor at a reagent flow rate of 4 mL min^{-1} and the production yield could reach nearly 5 grams per hour. Owing to the recognizable flower morphology, the interactions between cancer cells and silica–magnetic particles were easily identified, providing a convenient way to track the CTCs. In addition, the enhanced bioaccessibility achieved from the multilayered silica-magnetic microflower endows it with higher CTC capture rates toward tumor cell-spiked whole blood samples than commercial standard ferrofluid.[58] These preliminary studies demonstrated the superior screening performance of nonspherical materials over their spherical counterparts in simulated blood samples; however, real clinical blood samples from cancer patients should be further examined for revealing the practical roles of silica structures in liquid biopsy.

Besides the bioapplications discussed above, other applications of silica materials have also emerged in the past several years. For example, silver-decorated silica microspheres from a coaxial capillary device exhibited superior surface-enhanced Raman scattering activity for sensing benzenethiol, 2-naphthalenethiol, and 4-aminothiophenol at the nanomolar level;[96] silicon alkoxide cross-linked silica nanoparticle gel microspheres can be employed to encapsulate *E. coli* bacteria through a microfluidics emulsion system;[115] platinum-decorated silica nanospheres and silver-decorated silica nanofibers showed excellent catalytic activity for the oxidation of aldehyde and the reduction of 4-nitrophenol, respectively.[48,57] Given the unique advantages of microfluidics, especially precise spatio-temporal control, more broad applications are expected to be made with silica materials.

5. Key observations and future perspectives

The past decade has witnessed the emergence and unprecedented growth of microfluidics technology for silica materials synthesis. Compared to conventional batch synthesis systems, the unique features of microfluidics endow the resultant silica materials with more advanced physicochemical and biological properties. Microreactor-enabled controllable size, shape, porosity, and structure of silica materials help them find their niche in several bioapplication fields such as bioimaging, protein immobilization, bioadsorption, drug delivery, and liquid biopsy. To date, both material synthesis and biological applications established

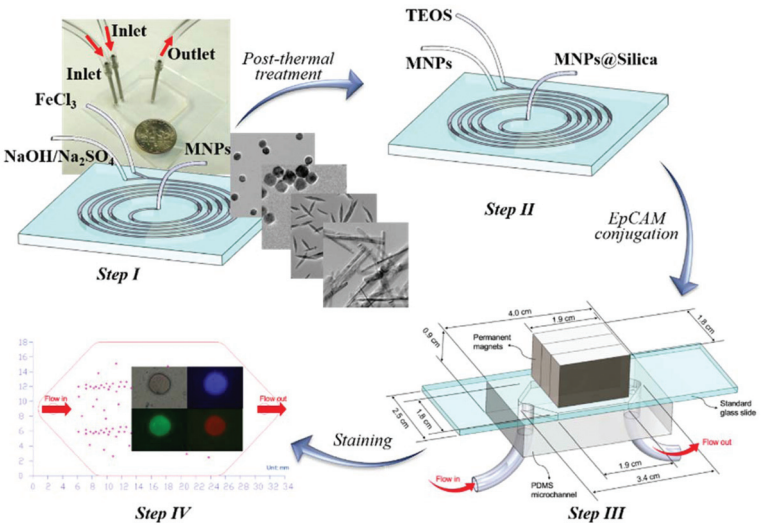

Fig. 15 Microfluidics synthesis of silica–magnetic nanomaterials for circulating tumor cell screening. Reproduced with permission from ref. 59.

based on laminar flow microreactors and discrete flow microreactors have provided encouraging results; however, there are still many pressing challenges that need to be adequately addressed.

First, low amount of production due to small operating volumes. Small operating volumes of reagents represent one of the biggest advantages of microfluidics reaction systems, which could significantly reduce reagent costs and waste generation during the screening of synthesis parameters. However, this limits the production quantities of silica materials to just gram-scale per hour currently, even when the fluid flow rate is set to milliliters per minute.[58] To solve this bottleneck, more rational design of microfluidics devices with parallel multiple modules that allow the handling of large volume of reagents should be developed for the scale-up synthesis of silica materials.[18]

Secondly, low diversity in particle properties. Microfluidics undoubtedly has outstanding capacities in tuning the size, shape, porosity, and structure properties of silica materials. However, as presented in Tables 2 and 3, most silica particle sizes range from a couple of hundred nanometers to several hundred micrometers; most silica materials developed to date have spherical shape and small pore size (less than 5 nm); and the structure of silica composites that mostly contain chitosan, gold or iron oxide is relatively simple. To enhance the biological performance of silica materials, nanosized, anisotropic, and multifunctional particles with a wide range of porosity should be developed.[9,11,125] This not only requires the improvement of microreactor designs, but also needs the concerted efforts of researchers from various disciplines such as chemistry, biology, and physics.

Thirdly, lack of inline control for real-time analysis. Full exploitation of microreactor synthesis systems needs real-time information about the chemical reaction progress for an immediate feedback control in the optimization of a product's physicochemical properties. Despite their merits in integration and automation, only very few microfluidics reaction systems have utilized inline analysis for materials synthesis;[126–129] even fewer cases are known for silica materials with no traceable optical, electronic, fluorescent, and magnetic properties. However, it is expected that, with the development of new miniaturized technological systems, more dedicated analysis tools can be integrated into microfluidics flow reactors for greatly increasing the depth of information available regarding the formation of silica particles.

Fourthly, insufficient demonstration of merits from microreactors over batch reactors. Most researchers have neglected the fact that microfluidics is not just an alternative to batch reactors; instead, it is a more advanced platform for the synthesis of silica materials. There have only been very few direct investigations to date showing the advanced merits of microreactors in terms of faster reaction kinetics, narrower particle size distributions, higher reproducibility, and larger application capacity.[41,43,44,46,54,60] More parallel studies are needed to examine the differences between microfluidics reactions and batch reactions.

Finally, but not lastly, simple and narrow range of applications. It is evident that, although versatile microreactor platforms and rich reaction methods have been developed for the synthesis of silica materials, their applications have lagged dramatically. Most of the applications mentioned above (*i.e.*, bioimaging, protein immobilization, bioadsorption, drug delivery, liquid biopsy, *etc.*) are still in the proof-of-concept stage. There is a long way from the laboratory to industrial/clinical practice, requiring convincing benchmarking and validation of the discoveries and techniques. Therefore, it is suggested that future studies on the rational design and synthesis of microfluidics-enabled silica biomaterials should be more application-oriented.

6. Conclusions

This paper provides a comprehensive review of the microfluidics-based development of silica materials with controllable size, shape, porosity, and structure properties, in particular, using laminar, segment, and droplet flow microreactors for a variety of biomedical applications. Despite great advances, microfluidics technology for the synthesis of silica biomaterials is still in its infancy. With rapid ongoing development of multiscale material design, sol–gel chemistry, microfabrication and microfluidics manipulation, silica materials with a more rational design for meeting specific bioapplication needs are expected to expedite soon. We envision that the versatility and advantages of microfluidics for silica materials synthesis could open new research frontiers and provide unparalleled opportunities for producing functional materials on demand with broad applications.

Conflicts of interest

There are no conflicts to declare.

Acknowledgements

The authors are grateful for the financial support from the National Institute of Health (NIH) Director's Transformative Research Award (R01HL137157), NSF ECCS-1509369, and NorrisCotton Cancer Center Developmental Funds (Pilot Projects).

References

1 W. Stöber, A. Fink and E. Bohn, *J. Colloid Interface Sci.*, 1968, **26**, 62–69.
2 C. T. Kresge, M. E. Leonowicz, W. J. Roth, J. C. Vartuli and J. S. Beck, *Nature*, 1992, **359**, 710–712.
3 C. Barbe, J. Bartlett, L. Kong, K. Finnie, H. Q. Lin, M. Larkin, S. Calleja, A. Bush and G. Calleja, *Adv. Mater.*, 2004, **16**, 1959–1966.

4 I. I. Slowing, B. G. Trewyn, S. Giri and V. S.-Y. Lin, *Adv. Funct. Mater.*, 2007, **17**, 1225–1236.
5 X. Du and J. H. He, *Nanoscale*, 2011, **3**, 3984–4002.
6 F. Q. Tang, L. L. Li and D. Chen, *Adv. Mater.*, 2012, **24**, 1504–1534.
7 N. Hao, K. Neranon, O. Ramström and M. Yan, *Biosens. Bioelectron.*, 2016, **76**, 113–130.
8 L. Tang and J. Cheng, *Nano Today*, 2013, **8**, 290–312.
9 N. Hao, L. F. Li and F. Q. Tang, *Int. Mater. Rev.*, 2017, **62**, 57–77.
10 N. Hao, L. Li and F. Tang, *Biomater. Sci.*, 2016, **4**, 575–591.
11 A. Albanese, P. S. Tang and W. C. W. Chan, *Annu. Rev. Biomed. Eng.*, 2012, **14**, 1–16.
12 I. I. Slowing, J. L. Vivero-Escoto, B. G. Trewyn and V. S.-Y. Lin, *J. Mater. Chem.*, 2010, **20**, 7924–7937.
13 N. Hao, L. F. Li and F. Q. Tang, *J. Biomed. Nanotechnol.*, 2014, **10**, 2508–2538.
14 C. Y. Mou and H. P. Lin, *Pure Appl. Chem.*, 2000, **72**, 137–146.
15 A. Abou-Hassan, O. Sandre and V. Cabuil, *Angew. Chem., Int. Ed.*, 2010, **49**, 6268–6286.
16 J. Il Park, A. Saffari, S. Kumar, A. Günther and E. Kumacheva, *Annu. Rev. Mater. Res.*, 2010, **40**, 415–443.
17 B. Sebastian and P. S. Dittrich, *Annu. Rev. Fluid Mech.*, 2018, **50**, 483–504.
18 G. M. Whitesides, *Nature*, 2006, **442**, 368–373.
19 N. Hao, Y. Nie and J. X. J. Zhang, *Int. Mater. Rev.*, 2018, **63**, 461–487.
20 W.-Y. Lin, Y. Wang, S. Wang and H.-R. Tseng, *Nano Today*, 2009, **4**, 470–481.
21 M. Lu, A. Ozcelik, C. L. Grigsby, Y. Zhao, F. Guo, K. W. Leong and T. J. Huang, *Nano Today*, 2016, **11**, 778–792.
22 D. Dendukuri and P. S. Doyle, *Adv. Mater.*, 2009, **21**, 4071–4086.
23 B. G. Chung, K.-H. Lee, A. Khademhosseini and S.-H. Lee, *Lab Chip*, 2012, **12**, 45–59.
24 L. Capretto, D. Carugo, S. Mazzitelli, C. Nastruzzi and X. Zhang, *Adv. Drug Delivery Rev.*, 2013, **65**, 1496–1532.
25 D. Baah and T. Floyd-Smith, *Microfluid. Nanofluid.*, 2014, **17**, 431–455.
26 W. Wang, M.-J. Zhang and L.-Y. Chu, *Acc. Chem. Res.*, 2014, **47**, 373–384.
27 A. M. Nightingale and J. C. de Mello, *J. Mater. Chem.*, 2010, **20**, 8454–8463.
28 T. W. Phillips, I. G. Lignos, R. M. Maceiczyk, A. J. DeMello and J. C. DeMello, *Lab Chip*, 2014, **14**, 3172–3180.
29 M. Rahman and E. Rebrov, *Processes*, 2014, **2**, 466–493.
30 E. Shahbazali, V. Hessel, T. Noël and Q. Wang, *Nanotechnol. Rev.*, 2014, **3**, 65–86.
31 T. M. Squires and S. R. Quake, *Rev. Mod. Phys.*, 2005, **77**, 977–1026.
32 N.-T. Nguyen and Z. Wu, *J. Micromech. Microeng.*, 2005, **15**, R1–R16.
33 C. T. Culbertson, S. C. Jacobson and J. Michael Ramsey, *Talanta*, 2002, **56**, 365–373.
34 Y. Song, J. Hormes and C. S. S. R. Kumar, *Small*, 2008, **4**, 698–711.
35 D. Mark, S. Haeberle, G. Roth, F. von Stetten and R. Zengerle, *Chem. Soc. Rev.*, 2010, **39**, 1153–1182.
36 H. Song, D. L. Chen and R. F. Ismagilov, *Angew. Chem., Int. Ed.*, 2006, **45**, 7336–7356.
37 J. H. Kim, T. Y. Jeon, T. M. Choi, T. S. Shim, S. H. Kim and S. M. Yang, *Langmuir*, 2014, **30**, 1473–1488.
38 S. Marre and K. F. Jensen, *Chem. Soc. Rev.*, 2010, **39**, 1183–1202.
39 S. A. Khan, A. Günther, M. A. Schmidt and K. F. Jensen, *Langmuir*, 2004, **20**, 8604–8611.
40 A. Günther, S. A. Khan, M. Thalmann, F. Trachsel and K. F. Jensen, *Lab Chip*, 2004, **4**, 278–286.
41 P. He, G. Greenway and S. J. Haswell, *Nanotechnology*, 2008, **19**, 315603.
42 A. Abou-Hassan, R. Bazzi and V. Cabuil, *Angew. Chem., Int. Ed.*, 2009, **48**, 7180–7183.
43 K. Shiba, K. Kambara and M. Ogawa, *Ind. Eng. Chem. Res.*, 2010, **49**, 8180–8183.
44 L. Gutierrez, L. Gomez, S. Irusta, M. Arruebo and J. Santamaria, *Chem. Eng. J.*, 2011, **171**, 674–683.
45 C. K. Chung, T. R. Shih, C. K. Chang, C. W. Lai and B. H. Wu, *Chem. Eng. J.*, 2011, **168**, 790–798.
46 P. He, G. Greenway and S. J. Haswell, *Chem. Eng. J.*, 2011, **167**, 694–699.
47 L. Gomez, M. Arruebo, V. Sebastian, L. Gutierrez and J. Santamaria, *J. Mater. Chem.*, 2012, **22**, 21420–21425.
48 S.-K. Lee, X. Liu, V. Sebastián Cabeza and K. F. Jensen, *Lab Chip*, 2012, **12**, 4080–4084.
49 N. Hassan, V. Cabuil and A. Abou-Hassan, *Angew. Chem., Int. Ed.*, 2013, **52**, 1994–1997.
50 S. Watanabe, T. Hiratsuka, Y. Asahi, A. Tanaka, K. Mae and M. T. Miyahara, *Part. Part. Syst. Charact.*, 2015, **32**, 234–242.
51 K. Shiba, T. Sugiyama, T. Takei and G. Yoshikawa, *Chem. Commun.*, 2015, **51**, 15854–15857.
52 T. N. Ng, X. Q. Chen and K. L. Yeung, *RSC Adv.*, 2015, **5**, 13331–13340.
53 A. Straß, R. Maier and R. Güttel, *Chem. Ing. Tech.*, 2017, **89**, 963–967.
54 N. Hao, Y. Nie, A. Tadimety, A. B. Closson and J. X. J. Zhang, *Mater. Res. Lett.*, 2017, **5**, 584–590.
55 Y. He, K.-J. Kim and C.-H. Chang, *Nanotechnology*, 2017, **28**, 235602.
56 Y. Nie, N. Hao and J. X. J. Zhang, *Sci. Rep.*, 2017, **7**, 12616.
57 N. Hao, Y. Nie and J. X. J. Zhang, *ACS Sustainable Chem. Eng.*, 2018, **6**, 1522–1526.
58 N. Hao, Y. Nie, A. Tadimety, T. Shen and J. X. J. Zhang, *Biomater. Sci.*, 2018, **6**, 3121–3125.
59 N. Hao, Y. Nie, T. Shen and J. X. J. Zhang, *Lab Chip*, 2018, **18**, 1997–2002.
60 N. Hao, Y. Nie, A. B. Closson and J. X. J. Zhang, *J. Colloid Interface Sci.*, 2019, **539**, 87–94.
61 N. Hao, Y. Nie, Z. Xu and J. X. J. Zhang, *J. Colloid Interface Sci.*, 2019, **542**, 370–378.

62 N. Hao, Y. Nie, Z. Xu, A. B. Closson, T. Usherwood and J. X. J. Zhang, *Chem. Eng. J.*, 2019, **366**, 433–438.
63 S. Venkataraman, J. L. Hedrick, Z. Y. Ong, C. Yang, P. L. R. Ee, P. T. Hammond and Y. Y. Yang, *Adv. Drug Delivery Rev.*, 2011, **63**, 1228–1246.
64 N. Hao, H. T. Chorsi and J. X. J. Zhang, *ACS Sustainable Chem. Eng.*, 2017, **5**, 2044–2049.
65 Y. Geng, P. Dalhaimer, S. S. Cai, R. Tsai, M. Tewari, T. Minko and D. E. Discher, *Nat. Nanotechnol.*, 2007, **2**, 249–255.
66 K. Yang and Y. Q. Ma, *Nat. Nanotechnol.*, 2010, **5**, 579–583.
67 E. Blanco, H. Shen and M. Ferrari, *Nat. Biotechnol.*, 2015, **33**, 941–951.
68 N. Hao, L. Li, Q. Zhang, X. Huang, X. Meng, Y. Zhang, D. Chen, F. Tang and L. Li, *Microporous Mesoporous Mater.*, 2012, **162**, 14–23.
69 N. Hao, L. F. Li and F. Q. Tang, *J. Mater. Chem. A*, 2014, **2**, 11565–11568.
70 N. Hao, H. H. Yang, L. F. Li, L. L. Li and F. Q. Tang, *New J. Chem.*, 2014, **38**, 4258–4266.
71 N. Hao, X. Chen, S. Jeon and M. Yan, *Adv. Healthcare Mater.*, 2015, **4**, 2797–2801.
72 N. Hao, F. Q. Tang and L. F. Li, *Microporous Mesoporous Mater.*, 2015, **218**, 223–227.
73 N. Hao, X. Chen, K. W. Jayawardana, B. Wu, M. Sundhoro and M. Yan, *Biomater. Sci.*, 2016, **4**, 87–91.
74 N. Hao, Y. Nie and J. X. J. Zhang, *Microporous Mesoporous Mater.*, 2018, **261**, 144–149.
75 J. A. Barreto, W. O'Malley, M. Kubeil, B. Graham, H. Stephan and L. Spiccia, *Adv. Mater.*, 2011, **23**, H18–H40.
76 Z. Gu, A. Biswas, M. X. Zhao and Y. Tang, *Chem. Soc. Rev.*, 2011, **40**, 3638–3655.
77 B. G. Trewyn, S. Giri, I. I. Slowing and V. S.-Y. Lin, *Chem. Commun.*, 2007, **43**, 3236–3245.
78 A. Stein, B. J. Melde and R. C. Schroden, *Adv. Mater.*, 2000, **12**, 1403–1419.
79 R. Seemann, M. Brinkmann, T. Pfohl and S. Herminghaus, *Rep. Prog. Phys.*, 2012, **75**, 016601.
80 S.-Y. Teh, R. Lin, L.-H. Hung and A. P. Lee, *Lab Chip*, 2008, **8**, 198–220.
81 S. A. Khan and K. F. Jensen, *Adv. Mater.*, 2007, **19**, 2556–2560.
82 I. Lee, Y. Yoo, Z. Cheng and H. K. Jeong, *Adv. Funct. Mater.*, 2008, **18**, 4014–4021.
83 M. Tachibana, W. Engl, P. Panizza, H. Deleuze, S. Lecommandoux, H. Ushiki and R. Backov, *Chem. Eng. Process.*, 2008, **47**, 1323–1328.
84 N. J. Carroll, S. B. Rathod, E. Derbins, S. Mendez, D. A. Weitz and D. N. Petsev, *Langmuir*, 2008, **24**, 658–661.
85 J. Il Park, Z. Nie, A. Kumachev, A. I. Abdelrahman, B. P. Binks, H. A. Stone and E. Kumacheva, *Angew. Chem., Int. Ed.*, 2009, **48**, 5300–5304.
86 D. Lee and D. A. Weitz, *Small*, 2009, **5**, 1932–1935.
87 D. Li, Z. Guan, W. Zhang, X. Zhou, W. Y. Zhang, Z. Zhuang, X. Wang and C. J. Yang, *ACS Appl. Mater. Interfaces*, 2010, **2**, 2711–2714.
88 W. Lan, S. Li, J. Xu and G. Luo, *Biomed. Microdevices*, 2010, **12**, 1087–1095.
89 V. Chokkalingam, B. Weidenhof, M. Krämer, S. Herminghaus, R. Seemann and W. F. Maier, *ChemPhysChem*, 2010, **11**, 2091–2095.
90 V. Chokkalingam, B. Weidenhof, M. Krämer, W. F. Maier, S. Herminghaus and R. Seemann, *Lab Chip*, 2010, **10**, 1700–1705.
91 M. Seo, I. Gorelikov, R. Williams and N. Matsuura, *Langmuir*, 2010, **26**, 13855–13860.
92 M. H. Lee, V. Prasad and D. Lee, *Langmuir*, 2010, **26**, 2227–2230.
93 S. Duraiswamy and S. A. Khan, *Nano Lett.*, 2010, **10**, 3757–3763.
94 A. Fang, C. Gaillard and J. P. Douliez, *Chem. Mater.*, 2011, **23**, 4660–4662.
95 W. Lan, S. Li, J. Xu and G. Luo, *Lab Chip*, 2011, **11**, 652–657.
96 H. Hwang, S.-H. Kim and S.-M. Yang, *Lab Chip*, 2011, **11**, 87–92.
97 J. S. Sander and A. R. Studart, *Langmuir*, 2011, **27**, 3301–3307.
98 W. Lan, S. Li, J. Xu and G. Luo, *Langmuir*, 2011, **27**, 13242–13247.
99 J. B. Wacker, I. Lignos, V. K. Parashar and M. A. M. Gijs, *Lab Chip*, 2012, **12**, 3111–3116.
100 W. Jeong, M. Choi, C. H. Lim and S. Yang, *Lab Chip*, 2012, **12**, 5262–5271.
101 W. Lan, S. Li, J. Xu and G. Luo, *Microfluid. Nanofluid.*, 2012, **13**, 491–498.
102 N. J. Carroll, P. F. Crowder, S. Pylypenko, W. Patterson, D. R. Ratnaweera, D. Perahia, P. Atanassov and D. N. Petsev, *ACS Appl. Mater. Interfaces*, 2013, **5**, 3524–3529.
103 D. Liu, B. Herranz-Blanco, E. Mäkilä, L. R. Arriaga, S. Mirza, D. A. Weitz, N. Sandler, J. Salonen, J. Hirvonen and H. A. Santos, *ACS Appl. Mater. Interfaces*, 2013, **5**, 12127–12134.
104 H. Zhao, J. Xu, W. Lan, T. Wang and G. Luo, *Chem. Eng. J.*, 2013, **229**, 82–89.
105 L. Shang, F. Shangguan, Y. Cheng, J. Lu, Z. Xie, Y. Zhao and Z. Gu, *Nanoscale*, 2013, **5**, 9553–9557.
106 M. T. Rahman, P. G. Krishnamurthy, P. Parthiban, A. Jain, C. P. Park, D. P. Kim and S. A. Khan, *RSC Adv.*, 2013, **3**, 2897–2900.
107 C. X. Zhao and A. P. J. Middelberg, *RSC Adv.*, 2013, **3**, 21227–21230.
108 M. Ju, X. Ji, C. Wang, R. Shen and L. Zhang, *Chem. Eng. J.*, 2014, **250**, 112–118.
109 H. Yan and C. Kim, *Colloids Surf., A*, 2014, **443**, 88–95.
110 Y. Cheng, C. Zhu, Z. Xie, H. Gu, T. Tian, Y. Zhao and Z. Gu, *J. Colloid Interface Sci.*, 2014, **421**, 64–70.

111 D. Liu, H. Zhang, E. Mäkilä, J. Fan, B. Herranz-Blanco, C. F. Wang, R. Rosa, A. J. Ribeiro, J. Salonen, J. Hirvonen and H. A. Santos, *Biomaterials*, 2015, **39**, 249–259.
112 D. Ferraro, Y. Lin, B. Teste, D. Talbot, L. Malaquin, S. Descroix and A. Abou-Hassan, *Chem. Commun.*, 2015, **51**, 16904–16907.
113 N. Hassan, A. Stocco and A. Abou-Hassan, *J. Phys. Chem. C*, 2015, **119**, 10758–10765.
114 L. Hou, H. Jiang and D. Lee, *Chem. Eng. J.*, 2016, **288**, 539–545.
115 J. J. Benson, L. P. Wackett and A. Aksan, *J. Microencapsulation*, 2016, **33**, 412–420.
116 J. Knossalla, S. Mezzavilla and F. Schüth, *New J. Chem.*, 2016, **40**, 4361–4366.
117 A. Larrea, A. Clemente, E. Luque-Michel and V. Sebastian, *Chem. Eng. J.*, 2017, **316**, 663–672.
118 J. Xu, W. Li, P. Shen, Y. Li, Y. Li, Y. Deng, Q. Zheng, Y. Liu, Z. Ding, J. Li and T. Zheng, *Microchim. Acta*, 2017, **184**, 3755–3763.
119 N. Bchellaoui, Z. Hayat, M. Mami, R. Dorbez-Sridi and A. I. El Abed, *Sci. Rep.*, 2017, **7**, 1–10.
120 R. Guo, X. T. Sun, Y. Zhang, D. N. Wang, C. G. Yang and Z. R. Xu, *J. Colloid Interface Sci.*, 2018, **530**, 465–472.
121 X. Cao, W. Li, Y. Fan and H. Dong, *Macromol. Chem. Phys.*, 2018, **219**, 1800106.
122 X. Zhao, Y. Liu, Y. Yu, Q. Huang, W. Ji, J. Li and Y. Zhao, *Nanoscale*, 2018, **10**, 12595–12604.
123 D.-Y. Kim, S. H. Jin, S.-G. Jeong, B. Lee, K.-K. Kang and C.-S. Lee, *Sci. Rep.*, 2018, **8**, 8525.
124 N. Hao and J. X. J. Zhang, *Sep. Purif. Rev.*, 2018, **47**, 19–48.
125 A. E. Nel, L. Mädler, D. Velegol, T. Xia, E. M. V. Hoek, P. Somasundaran, F. Klaessig, V. Castranova and M. Thompson, *Nat. Mater.*, 2009, **8**, 543–557.
126 I. Lignos, S. Stavrakis, A. Kilaj and A. J. DeMello, *Small*, 2015, **11**, 4009–4017.
127 B. Swain, M. H. Hong, L. Kang, B. S. Kim, N. H. Kim and C. G. Lee, *Chem. Eng. J.*, 2017, **308**, 311–321.
128 S. Krishnadasan, J. Tovilla, R. Vilar, A. J. DeMello and J. C. DeMello, *J. Mater. Chem.*, 2004, **14**, 2655–2660.
129 A. Toyota, H. Nakamura, H. Ozono, K. Yamashita, M. Uehara and H. Maeda, *J. Phys. Chem. C*, 2010, **114**, 7527–7534.